8-2018

Mapping Lower Austin Chalk Secondary Porosity Using Modern 3-D Seismic and Well Log Methods in Zavala County, Texas

David Kilcoyne
University of Arkansas, Fayetteville

Mapping Lower Austin Chalk Secondary Porosity Using Modern 3-D Seismic and Well Log Methods in Zavala County, Texas

A thesis submitted in partial fulfillment
of the requirements for the degree of
Master of Science in Geology

by

David Joseph Kilcoyne
University College Cork
Bachelor of Science in Geoscience, 2016

August 2018
University of Arkansas

This thesis is approved for recommendation to the Graduate Council.

_____
Christopher L. Liner, PhD
Thesis Director

_____
Thomas A. McGilvery, PhD
Committee Member

_____
Robert Liner, M.S.
Committee Member

Abstract

Establishing fracture distribution and porosity trends is key to successful well design in a majority of unconventional plays. The Austin Chalk has historically been referred to as an unpredictable producer due to high fracture concentration and lateral variation in stratigraphy, however recent drilling activity targeting the lower Austin Chalk has been very successful. The Upper Cretaceous Austin Chalk (AC) and underlying Eagle Ford (EF) units are considered by many to act as a single hydrocarbon system, with communication between these two units largely through expulsion or dewatering fractures, extensional faults or along the AC/EF unconformity. Total porosity for the Eagle Ford is composed of a primary matrix component and secondary fracture porosity. For the Austin Chalk, the secondary porosity includes both dissolution and fracture components which complicate wireline and seismic interpretation.

The current study interprets 40 square miles of modern 3D seismic data for horizons and faults using amplitude, coherence, curvature and ant tracking seismic attributes. Post stack acoustic impedance (AI) inversion is applied to the time migrated seismic volume with control from two wells; this input data is similar to that available to independent operators active in the area. Wireline acoustic impedance plotted against sonic and neutron-density porosity respectively, reveals strong correlations that allow calibration of seismic AI into primary, secondary and total porosity from which time slices and surface maps are created. Relationships are identified between porosity and geological features of interest, such as faulted and brittle zones, that may prove useful in guiding future well development in the lower Austin Chalk.

Acknowledgements

I would like to thank my advisor, Dr. Christopher Liner, for his advice, guidance and continued support during my time at the University of Arkansas. I would also like to thank my other committee members, Dr. Thomas (Mac) McGilvery and Robert Liner, for their insight and suggestions. I am also grateful to the Department of Geoscience of the University of Arkansas for giving me the opportunity to pursue a Master's degree as well as financial support as a teaching assistant. I would like to thank Stephens Production Company for their donation of the data used in this investigation, Schlumberger for their donation of Petrel and Techlog, and CGG for use of HampsonRussell.

To my parents, thank you for helping me be where I am today.

Table of Contents

Introduction

The Austin Chalk (AC) continues to produce over a century after its initial hydrocarbon potential was discovered (Udden and Bybee, 1916). The original subsurface traps were igneous in nature with drilling focused on, and in the area immediately surrounding, volcanic centers ('serpentine plugs') embedded within the AC and overlying Anacacho Limestone. Over 50 million bbls of oil and significant gas production is documented from these serpentine plugs across south Texas, including the Uvalde Volcanic Field, centered in Zavala County, where over 150 volcanic plugs have been identified (Ewing and Caran, 1982; Mathews, 1986). Jenny (1951) and Ewing and Caran (1982) discuss initial magnetic and seismic methods used to identify these traps, while remote sensing, both aerial and land magnetic surveys, in addition to geochemical studies were used to map the volcanic centers. In the 1970's and '80's the south Texas volcanic play began to reach maturity and, with a substantial rise in oil prices during the 1973 Oil Embargo, drillers transitioned to targeting other stratigraphic and structural features in the Late Cretaceous deposits, including vertical fractures in the heavily deformed AC (Haymond, 1991).

The Austin Chalk quickly earned a reputation as an unpredictable producer due to a poor stratigraphic and structural understanding. Dry wells or wells with rapid production decline were common when the frac ture system was missed because the AC is a low porosity, low permeability carbonate reservoir with a dual porosity system (Pearson, 2012). Local increases in AC porosity can be attributed to both deformational and dissolution processes. As the focus shifted from targeting igneous plugs to vertical fractures, the AC became one of the first plays to utilize horizontal drilling. Kuich (1989) identifies the key role of horizontal drilling, where he correlates greater production with greater number of vertical fractures intercepted in the Giddings Field. This is supported by Schnerk and Madeen (2000), although they qualify this statement indicating that

fractures extending beyond the unit tend to be either leaky or water-bearing due to significant water in the middle AC.

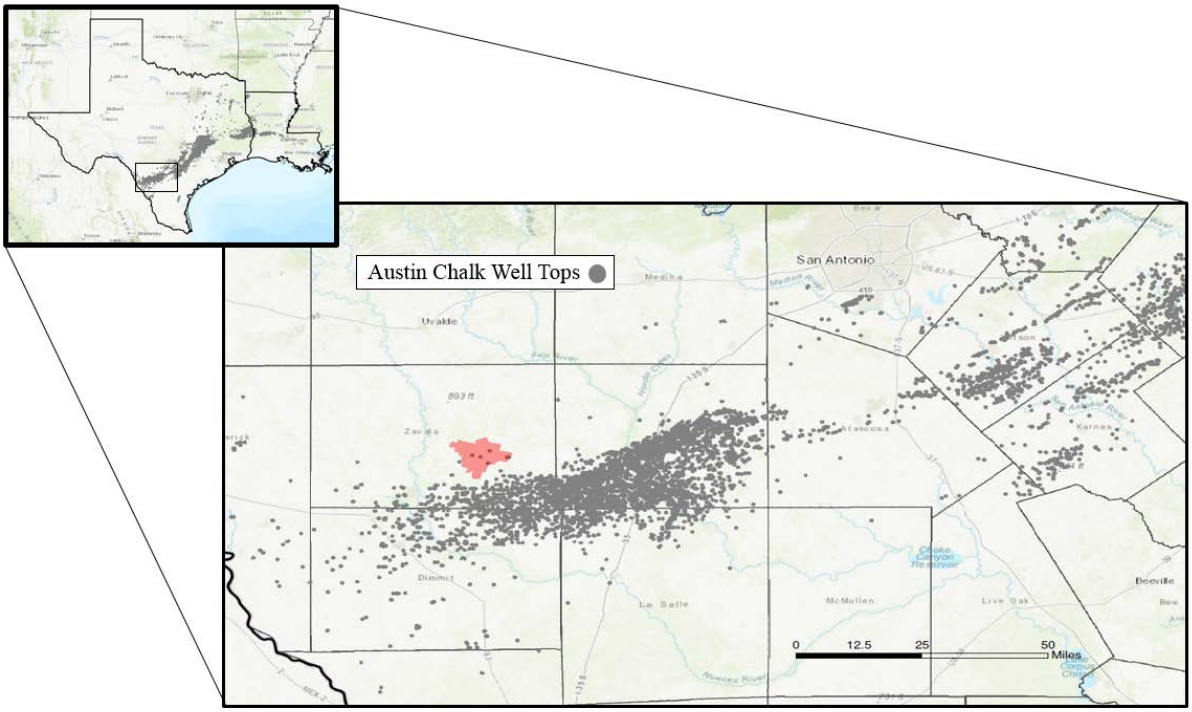

Figure 1. Reference map of southwest Texas, showing the seismic survey in red. Grey points represent well tops of both vertical and horizontal wells targeting Austin Chalk reservoirs. The survey sits several miles north of the Pearsall Field, located in Frio County and extending to the southwest into south Zavala and northern Dimmit County, where significant production from the AC has been recorded. The inset map shows interest in the AC extends beyond the Pearsall Field, right through south Texas and into Louisiana.

The source rock potential of the Austin Chalk is discussed by many authors, including Grabowski (1984) where the Lower AC is identified as organic rich, albeit with less abundance and less consistent distribution than the underlying Eagle Ford (EF). Grabowski (1984) further documents the variability of organic material abundances including significant lateral and vertical variation. Hinds and Berg (1990) classified the source rock maturity of Late Cretaceous Gulf Coast deposits in 3 categories: 1) immature (depths of less than 6,000 ft.), 2) zone of accumulation (depths of 6-

7,000 ft.), where commercial quantities of hydrocarbons are generated and remain in place within matrix porosity, and 3) mature (depths greater than 7,000 ft.), where hydrocarbons have been generated in place and expelled into nearby fractures.

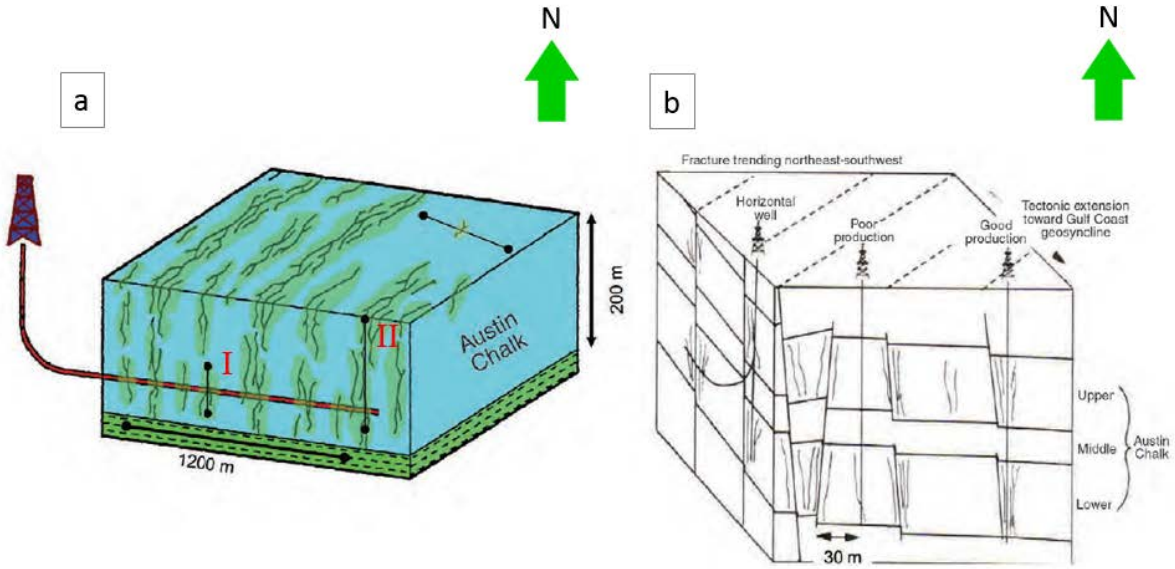

Figure 2 Schematic of the typical play in the Austin Chalk in west Texas, modified from Chopra and Marfurt (2007). (a) Shows a horizontal well bore intersecting near vertical fractures. Fractures restricted to the Lower Austin Chalk (I) typically contain hydrocarbons, while fractures extending beyond the Lower AC (II) can be water bearing or leaky. (b) Demonstrates the relationship between production and different geologic features in the AC. The development of horizontal drilling and improved seismic imaging has allowed greater drilling accuracy and better resolution of subsurface targets.

Organic-rich mudrocks of the Eagle Ford have been noted in the literature since Ferdinand Roemer observed 'black shale with fish fossils' in 1852. Until recently, the majority of EF research has focused on outcrop studies (e.g. Stephenson et al, 1942; Adkins and Lonzo, 1951) with significant lithological differences observed in the EF between the Rio Grande Embayment, San Marcos Arch and East Texas Basin as far back as 1932. Historical subsurface investigations of the EF in south Texas were limited, with the earliest published subsurface correlation produced by Winter (1961)

whose primary interest was the overlying Austin Chalk. Following increased interest in the AC in the 1970's, Grabowski's (1984) work on the Austin Chalk produced early Eagle Ford subsurface correlations based on a Cenomanian lower member and Turonian upper member. This is where the EF was first subdivided into a lower and upper unit, based on GR. The EF was the focus of continued interest, with Dawson (2000) utilizing core data from La Salle County to define 6 regionally persistent Eagle Ford microfacies, emphasizing the stratigraphic variability in the unit.

Following the emergence of unconventional reservoirs, the EF has received notably more attention over the past decade than in its previous history. As an unconventional reservoir, the EF of southwest Texas is an attractive target compared with other shale plays due to a reduced clay and greater carbonate content, making it more brittle. Following rapid development, significant research has been recently produced that better characterizes its depositional setting and TOC distribution (e.g. Harbour, 2011), subsurface extent (Hentz and Ruppel, 2010) and other parameters (e.g. Treadgold et al., 2013; Chen et al., 2015).

The current research involves interpretation of a 3D seismic survey referred to as the Pedernales survey, with a focus on the Lower Austin Chalk. Published structure maps (e.g. Martin et al., 2011) indicate the Lower AC of south-east Zavala County is situated in both the immature and zone of accumulation of the Hinds and Bergs (1990) classification meaning in some areas, hydrocarbons potentially could have been generated within the AC or have migrated from the Eagle Ford.

Differentiating the origin of hydrocarbons in fractures zones has been historically difficult as both the AC and EF predominantly contain Type II kerogen (Pearson, 2010). Detailed geochemical analysis carried out by Robison (1997) determined both formations contain intervals rich in TOC capable of generating commercial quantities of hydrocarbons. It was also noted that the Eagle Ford rocks 'not only exhibit greater organic carbon content, but also have greater quantities of oil-prone

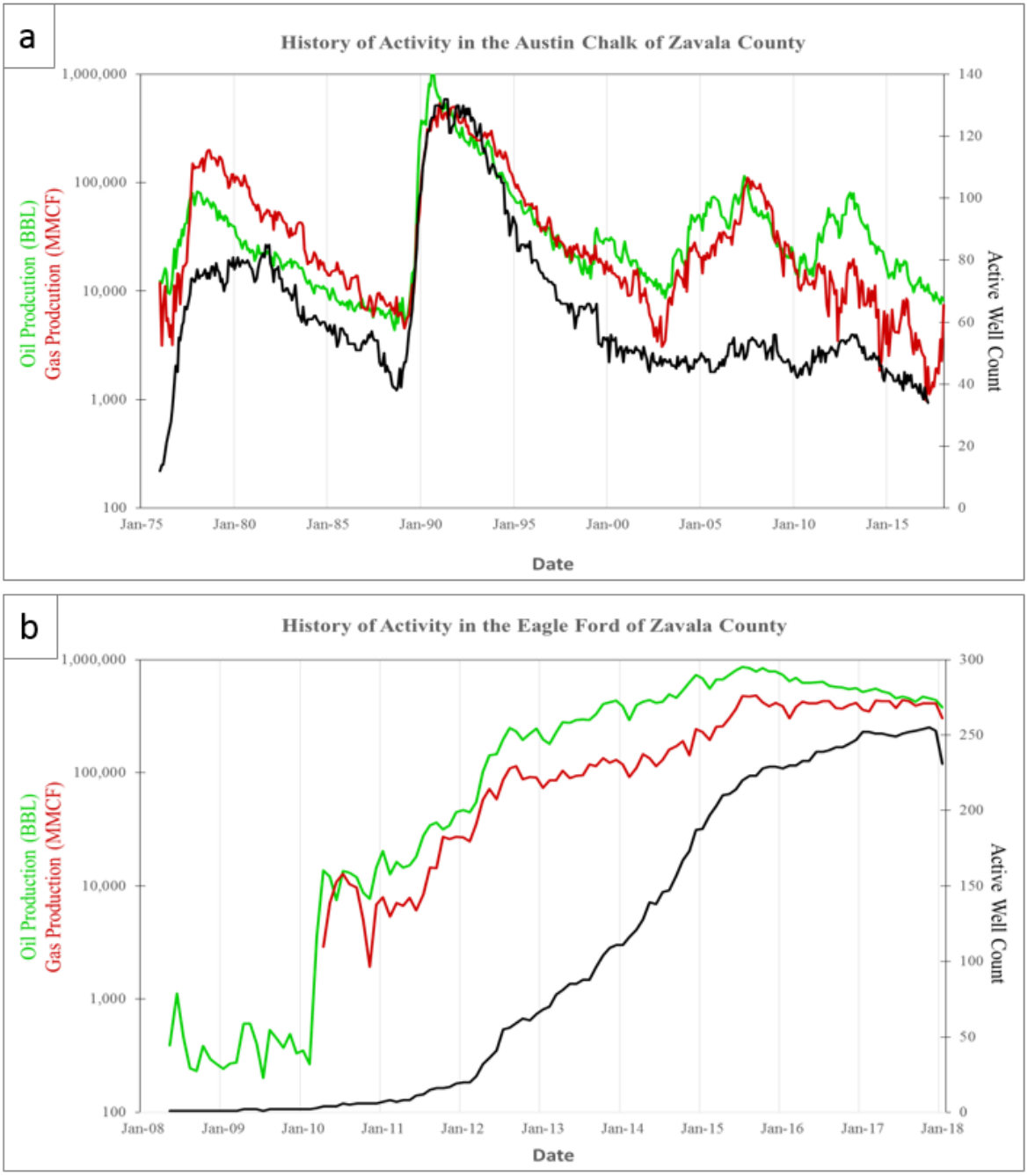

Figure 3. Monthly production history from Zavala County taken from DrillingInfo (2018), (a) Production from the Austin Chalk in Zavala County shows big increases in the 70s and 90s correlating with the Oil Embargo and onset of horizontal drilling. In the years following the early 90s there is significant decoupling between production and active well count, most likely brought on by improved completion methods. (b) An initial rapid interest in the Eagle Ford appears to plateau in late 2015 in Zavala County.

kerogen (fluorescent amorphinite and exinite) when compared with rocks from the Austin Chalk' (Robinson, 1997, p. 287).

As a result, the EF is considered the dominant source of hydrocarbons in fractured zones of the Austin Chalk, with oil generation in the early Miocene and vertical migration through fractures to charge AC reservoirs (Pearson, 2012).

Five wells have been drilled within the survey area targeting the AC since 1990, applying both horizontal and vertical drilling. All wells are reported dry, even in the most recent attempts of 2010 using more advanced technology. However, considerable success has been observed in the underlying Eagle Ford and all other Gulfian units within the survey area, giving optimism that there may be overlooked hydrocarbon potential in the AC. Such well tops will be used to generate an advanced velocity model in Petrel to convert the data to the depth domain

Due to the history of production in the AC over the last century, production from all other Gulfian units (Figure 4) across south Texas, and rapid development of the EF over the last decade, substantial work has already been carried out on the Late Cretaceous rocks of the Gulf Coast with respect to structure, stratigraphy and geochemistry. Regionally, several published investigations document the use of both deterministic and stochastic inversions of pre-and post-stack data to estimate rock properties of the Lower Gulfian south Texas units. The majority of such investigations are more recent and focused on the EF, targeting rock properties including brittleness, porosity and organic richness (e.g. Treadgold et al., 2011; Kumar et al., 2014).

A similar study to this investigation was carried out by Ogiesoba and Eastwood (2013) on the Lower AC (LAC), also using a post stack 3D seismic survey and seismic inversion. Their study was conducted in Dimmit County, approximately 30 miles south of the Pedernales survey, at a

setting about 1000 ft deeper. Results of the current study will be compared to Ogiesoba and Eastwood's (2013) work.

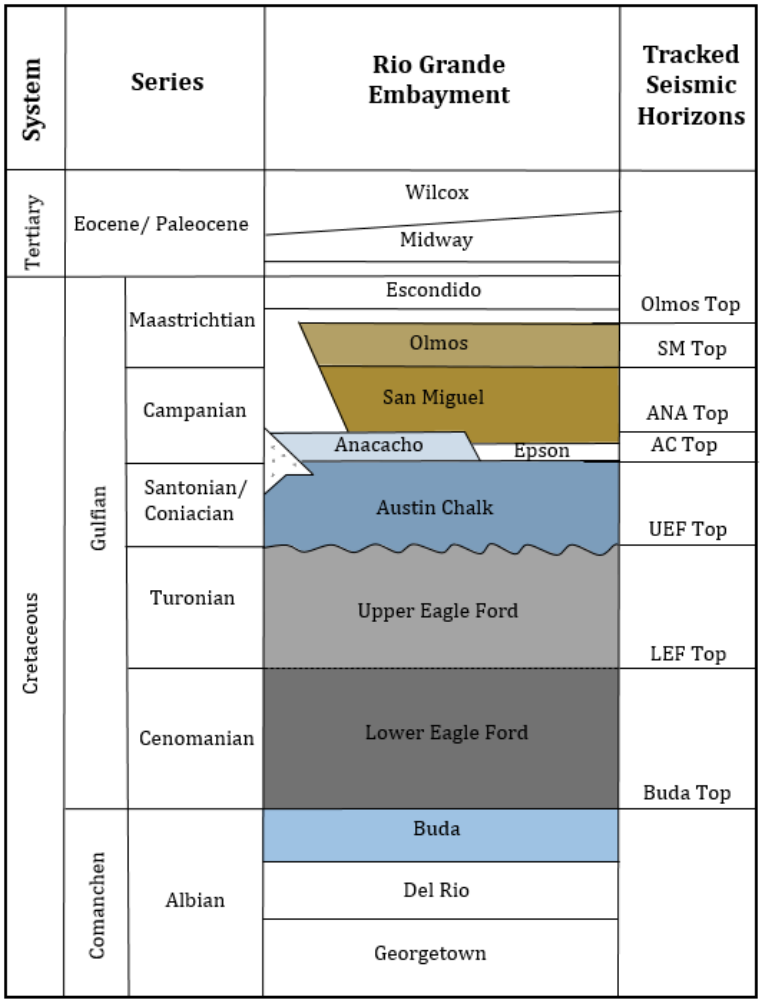

Figure 4. Stratigraphic column of relevant Cretaceous units in the Rio Grande Embayment, modified from Condon and Dyman (2003). Colors correspond to geoseismic section in Figure 5.

The Pedernales 3D seismic dataset was also used by Bennett (2015) to identify and interpret Late Cretaceous volcanic mounds. Although Late Cretaceous features were identified, the nature of this study is much narrower, focused exclusively on the Lower AC and relevant EF features. Smirnov

(2018) also utilizes this dataset to conduct a similar study on fractures in the deeper Early Cretaceous Buda Limestone.

The purpose of this research is to test the hypothesis that a post stack seismic survey can be used to map fractured areas in the Austin Chalk using sparse well control. A similar methodology to Doldberg et al. (2000) will be applied, where sonic porosity and neutron-density porosity logs are calibrated into an acoustic impedance volume and used to estimate matrix and total porosity, respectively. Porosity of the AC is composed of a primary matrix component with secondary porosity associated to fractures and/or dissolution. Seismic attributes that highlight discontinuities, including amplitude, curvature, variance, ant tracking and attenuation are suitable for this project. Post stack acoustic impedance (AI) volumes were generated to extract lithological and structural properties including porosity, brittleness and potential fracture zones. Identification of these properties is crucial since two current plays in the AC rely heavily on these parameters; horizontal wells that target vertical to sub-vertical fractured rocks and horizontal wells that target tight TOC-rich benches in the chalk that require hydraulic fracturing.

Due to a lack of success targeting the Upper Austin Chalk the lower interval was selected to be investigated in Zavala County. Traditionally, fractures in the Upper AC were targeted in the Pearsall Field and Lower AC fractures in the Giddings Field (Hovorka and Nance, 1994). Investigating the basal AC of the Pearsall Field, Ogiesoba and Eastwood (2013) determined 90% of productive zones in the Lower AC in north Dimmit County are associated with EF vertical en-echelon faults. However, this study sits north of the traditional AC production belt. With extensive 3D seismic survey coverage and well log data collected over the last decade targeting the underlying EF, the Lower AC could be a viable hydrocarbon play for many small to medium operators taking advantage of the stacked play opportunity.

Geologic Setting

The Texas Gulf Coast is a structurally complex history that has been comprehensively reviewed by Ewing (1991), Salvador (1991) and Dawson et al. (1995). In addition, Bennett (2015) provides a good reference for the stratigraphic and tectonic evolution of all Late Cretaceous deposits of south east Zavala County. A condensed discussion of the geologic setting is provided with a focus on the relevant Lower Gulfian units.

Tectonic Setting

The Gulfian units of Zavala County were deposited on the drowned Early Cretaceous Comanche Platform along the Cretaceous northwest margin of the Gulf of Mexico Basin (GoMB) (Condon and Dyman, 2003). The orientation of the Early Cretaceous Platform dictated the northwest-southeast orientation of all Late Cretaceous units. There were three dominant structural regions on the Late Cretaceous GoMB margin (Figure 6): the Rio Grande Embayment, Houston Embayment and the East Texas Basin.

The Rio Grande Embayment is a structurally negative feature separated from the Houston Embayment and the East Texas basin by the San Marcos Arch (Condon and Dyman, 2003). This arch is a subsurface extension of the Llano uplift that extends southeast ward, with several Jurassic and Cretaceous units absent over the arch (Pearson, 2012). The embayment is bounded to the north by the Ouachita orogenic belt, to the northeast by the San Marcos Arch, and to the south by the upper Cretaceous Sligo Reef Margin. The Rio Grande Embayment extends southwesterly into northern Mexico. The Maverick Basin is a sub-division of the Rio Grande Embayment and is found in only the most south western counties of Texas (Scott, 2004), with the Pedernales seismic survey located on the perimeter of the sub-basin.

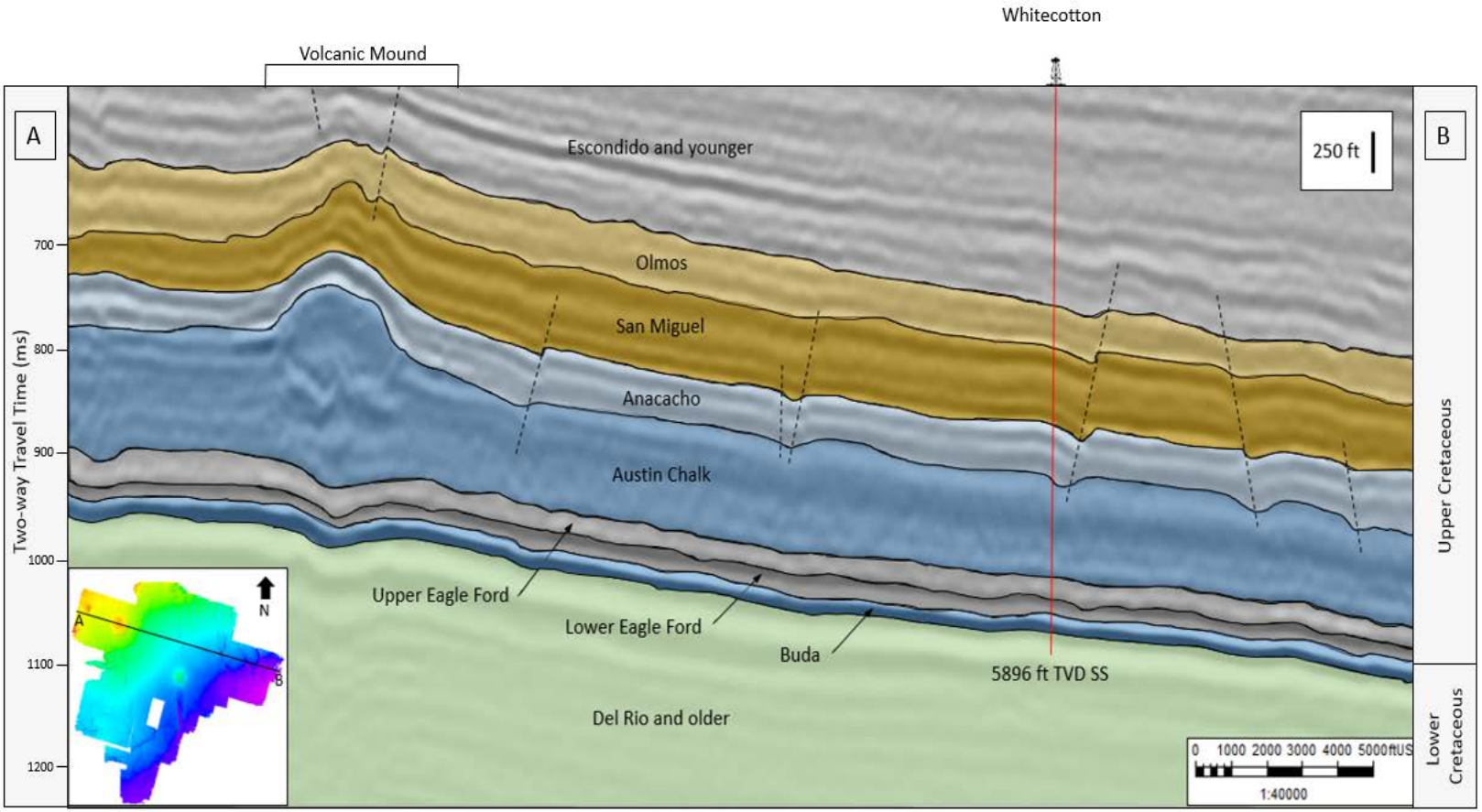

Figure 5 shows volcanic mound development in the Upper Austin Chalk, with velocity drawdown directly beneath the mound in the Lower Austin Chalk and the older units. Faulting is more prevalent in the younger Gulfian units, however no clear offset was seen on the Lower Austin Chalk reflector.

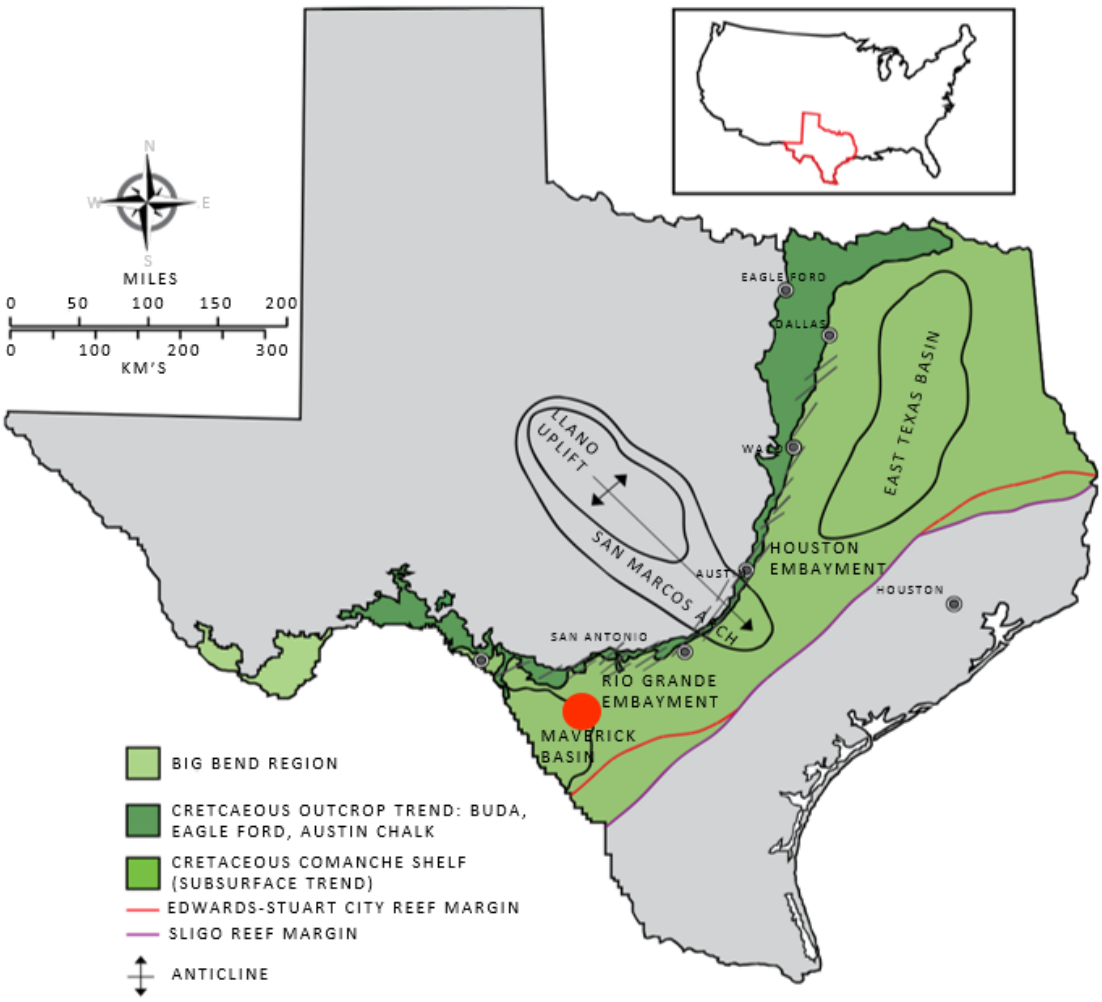

Figure 6. Map demonstrating the northwest to southeast trend of the Early Cretaceous Comanche Shelf, with major structural settings labelled. The Maverick Basin developed as a failed rift arm during the opening of the GoMB in the Jurassic. Thicker stratigraphic sections are observed in the Maverick Basin than the rest of the Rio Grande Embayment due to increased accommodation space, modified from Bennett (2016).

The Balcones fault system (Figure 7) of south Texas runs parallel to the Ouachita orogenic belt (Mathews, 1986). It is defined as a series of down to the south and south normal faults with displacements that can exceed 1600 ft against basement rocks of Paleozoic age (Condon and

Dyman, 2003). The Luling fault zone lies parallel to, and southeast of, the Balcones fault zone. These faults are normal and have down-to-the-northwest (opposite to the displacements of the Balcones faults) ranging from about 1,000 to 2,000 ft. The combined Balcones-Luling faults bound a broad down-dropped graben (Condon and Dyman, 2003) approximately 250 miles in length and was the location of significant volcanic activity, including the previously mentioned Uvalde Volcanic Field. Differential compaction due to ash deposition and radial faulting is associated with the volcanic features during deposition of the Austin Chalk and Anacacho Limestone (Ewing and Caran, 1982).

Stratigraphy

Upper Cretaceous stratigraphy varies across south Texas due to the different depositional environments and various structural settings. This research is focused on Zavala County in southwest Texas, so the stratigraphy of the Maverick Basin is discussed.

Lower Eagle Ford

The Lower EF (LEF) is a transgressive marine interval dominated by laminated, organically rich shales deposited after the Mid-Cretaceous Unconformity (MCU) (Dravis, 1979). It is a dark-gray mudrock and locally developed light-gray calcareous mudrock, marl and possible limestone, deposited conformably atop the Buda Formation which is a shallow platform lime mudstone (Hentz and Ruppel, 2010). Only in the Maverick Basin is the EF typically divided in two separate lithological units, termed the Upper and Lower Eagle Ford (Grabowski, 1984). The LEF was deposited during one of two global oceanic anoxic events (OAE), where widespread source rock deposition was common (Schlanger et al., 1976).

Lower Eagle Ford total organic content is the highest of all Lower Gulfian Units, owing to the OAE occurring during its deposition. Dawson (2000) reports average TOC values of 2.8 wt.%, and maximum values of 6.8 wt.% in the Getty J. T. Wilson #1 well in nearby La Salle County. Martin et al. (2011) report average water saturation values of 34%.

Upper Eagle Ford

The Upper EF (UEF) is an interbedded calcareous mudrock deposited during a regressive highstand (Hentz and Ruppel, 2010). Material was deposited in shallower water depths than that of the Lower EF owing to the beginning of a regressive cycle. Higher carbonate and fossil content are seen in the UEF, as a consequence of decreasing water depth (Dawson, 2000), to such an extent that in certain locations it can be difficult to discern the boundary of the Austin Chalk and the Eagle Ford.

Due to poor preservation conditions, TOC values are less in the Upper Eagle Ford than in its lower counterpart (Treadgold et al., 2011). Water saturation is also greater in the UEF, with an average value of 56% (Martin et al., 2011).

Austin Chalk

The Austin Chalk consists of recrystallized, fossiliferous, interbedded chalks, marls, and black shales (Hinds and Berg, 1990) and lies paraconformably above the Upper Eagle Ford (Ewing and Caran, 1996). Deposited during a regressive cycle on a gently sloping marine shelf in water depths of ranging from 30-300 ft (Pearson, 2012), the uppermost section of the AC is often interbedded with volcanic ash. The AC is typically subdivided into 3 lithological units (Hovorka and Nance, 1994); the upper and lower unit comprised of interbedded chalk and marl separated by a marl-dominant middle unit. The AC can also be subdivided into 3 similar mechanical units (Corbett et

al., 1987). The upper and lower units contain less clay and are therefore more brittle, leading to higher fracture density and improved reservoir quality (Hovorka and Nance, 1994).

Regionally, the AC is described in the literature in terms of updip or downdip facies, with a present depth of 5,000 ft used to differentiate the two regions (Ogiesoba and Eastwood, 2013). The majority of the AC in seismic coverage is located downdip using this classification. The AC is darker, less fossiliferous, and less bioturbated in these areas, having been deposited below wave base in outer-shelf and upper-slope environments in nearly anoxic conditions (Grabowski, 1984; Dawson et al., 1995). TOC can be as high as 3.5% in down dip regions.

Up dip Austin Chalk deposition occurred in a shallow marine shelf with normal marine conditions resulting in lower organic preservation (Grabowski, 1984; Dawson et al., 1995). Both stratigraphically and there is significant variation, particularly in TOC distribution (Grabowski, 1984).

Austin Chalk matrix porosity values are a function of depth, mostly ranging from 3-9% (Dawson et al., 1995). However higher values are observed locally owing to fracture development. Unfractured Austin Chalk permeability averages between 0.02-1.27 mD, but like porosity can be substantially larger locally due to fracture development (Martin et al., 2011).

Varying porosity values reported across the AC trend are associated with burial history, exposure to tectonic faulting and environmental setting. Matrix porosity shows an expected general trend of decrease with depth of burial between 1,000 and 8,000 ft across south Texas (Dravis, 1979). The subsurface AC underwent porosity loss due to 3 main processes; mechanical compaction, burial stabilization of primary aragonite material and associated cementation and pervasive pressure solution and cementation (Scholle, 1977; Dravis (1979).

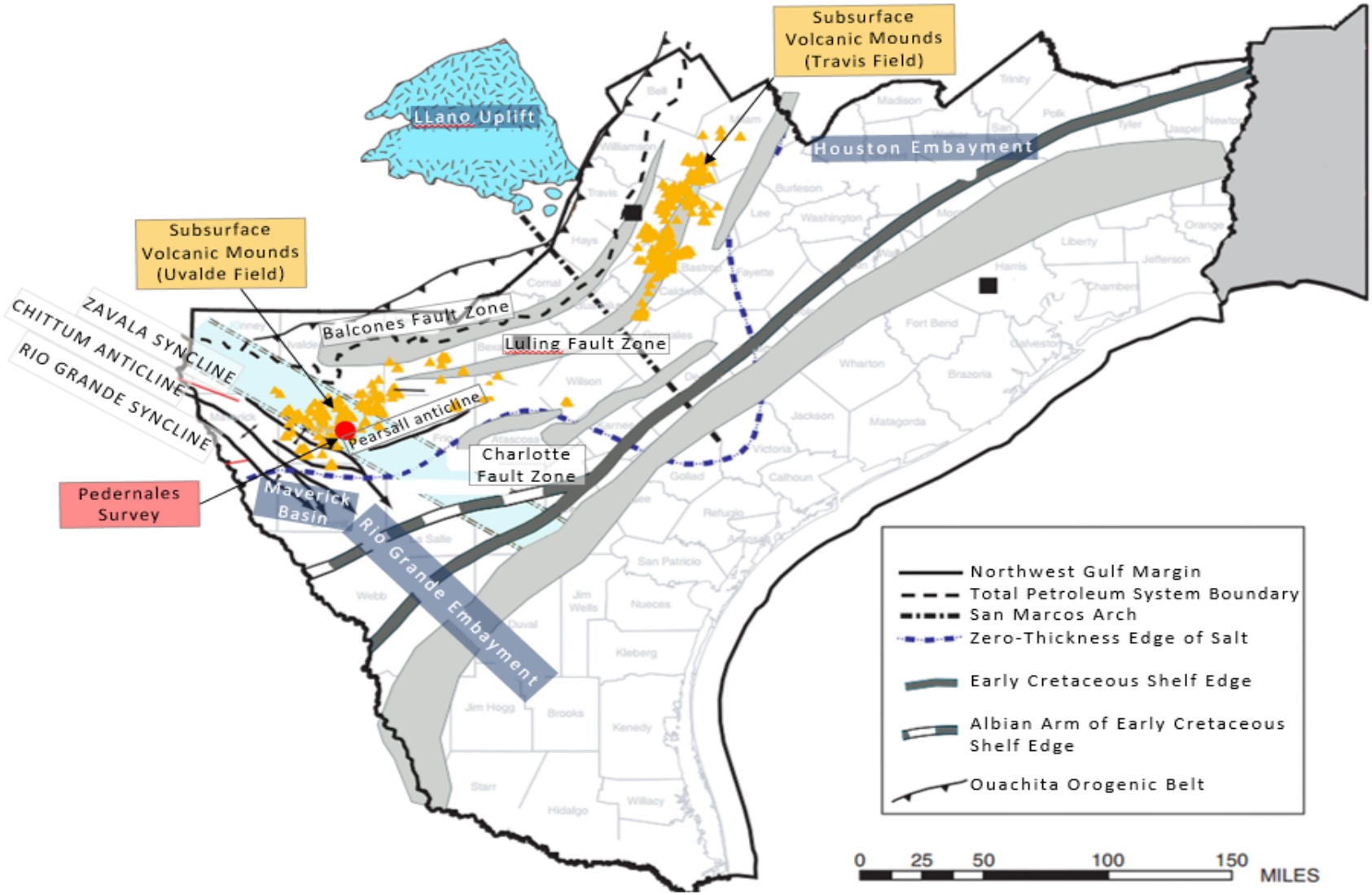

Figure 7. South Texas structural map showing major structural features. The survey area is positioned within the Uvalde Volcanic Field and very near the Pearsall anticline (modified from Condon and Dyman, 2003).

Deposition and Tectonic Evolution

Deposition of Lower Gulfian units in the Maverick basin were heavily influenced by structural activity prior to the Late Cretaceous, including the breakup of the Precambrian supercontinent, the Ouachita orogeny and the breakup of Pangea (Salvador, 1991). The Ouachita orogeny resulted in north-south trending folds of Early Paleozoic rock in the Permian, one such uplift being the Llano uplift (Condon and Dyman, 2003; Salvador, 1991).

As Pangea broke apart in the Late Triassic, rift zones began to develop across North America, one such zone was situated in the Rio Grande Embayment (Jacques and Clegg, 2002). The Balcones and Lulling fault zones developed in the Late Triassic through continued extension of these systems.

The Gulf of Mexico opened in the Late Jurassic, an event that has been well documented in the literature (e.g. Salvador, 1991; Tyler and Ambrose, 1986). At this time, the Maverick Basin developed as a failed rift arm of the Gulf of Mexico setting up a series NW-SE trending half-graben features throughout the remainder of the Jurassic (Scott, 2004).

The Early Cretaceous was a time of relative tectonic stability (Salvador, 1991) when the Rio Grande Embayment developed as a structurally negative feature owing to thermal subsidence. Continued fault growth and salt withdrawal allowed the Maverick Basin to develop as a sediment depocenter by the beginning of the Late Cretaceous (Bennett, 2015).

The Eagle Ford was the first Lower Gulfian unit to be deposited (Cenomian-Turnonian), during which the Western Interior Seaway was connected to the Gulf of Mexico. Sediment deposition was not consistent across the Cretaceous NW GoM margin. In the LEF, decreasing clay content and increasing carbonate content is seen with distance westward from the San Marcos Arch (Hentz

and Ruppel, 2010). Elevated TOC levels, increased pyrite concentration and a lack of burrowing (Harbor, 2011) all support anoxic conditions reported at that time. Trends of increasing TOC with distance from the structural high were also observed (Harbour, 2011).

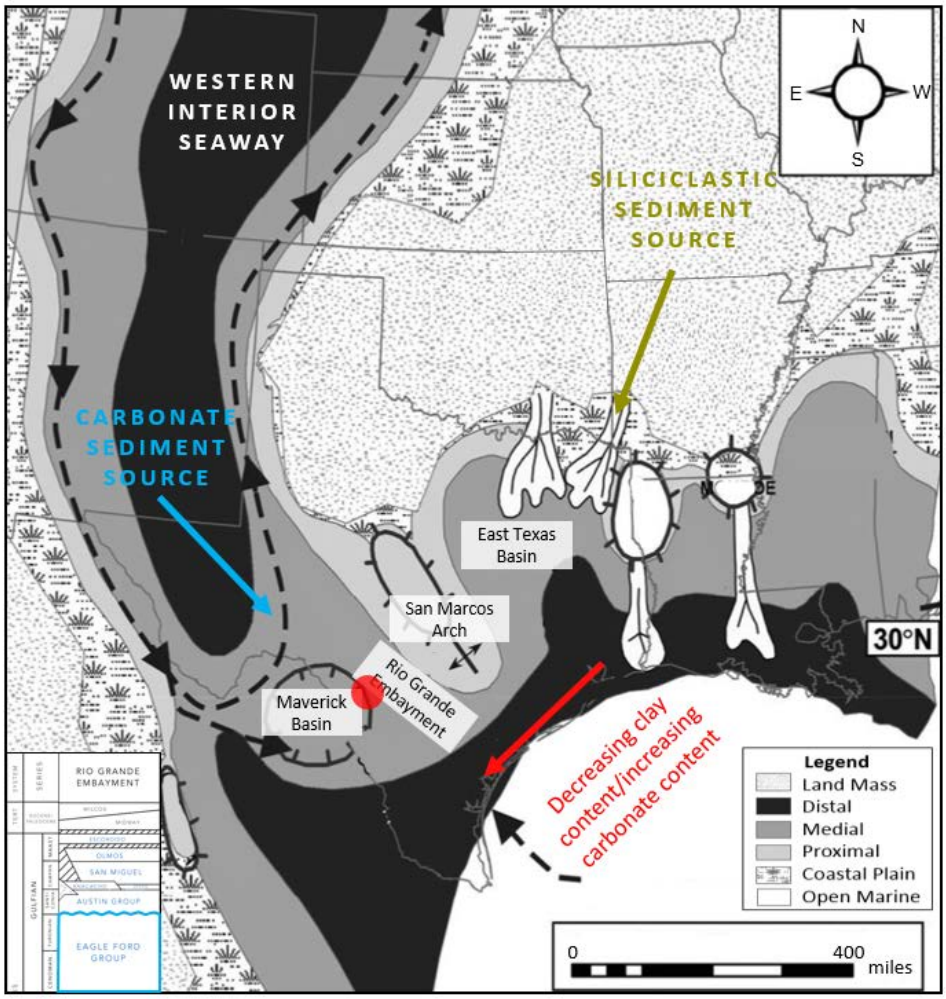

Figure 8. Shows Late Cenomanian depositional settings, modified from Hentz and Ruppel (2011). Increased siliciclastic content is seen in the East Texas Basin and Houston Embayment attributed to sediment carried in run off from the continent. This siliciclastic material is largely absent in the Rio Grande Embayment as a result of the structural high San Marcos Arch. Carbonate content increases in the Rio Grande Embayment with distance from the San Marcos Arch.

The Eagle Ford depositional sequence consists of a retrogradational lower unit and a progradational upper unit, which are interpreted as transgressive and highstand deposits respectively. The Cenomanian-Turonian stage boundary occurs at or near the maximum flooding surface which separates these members (Condon and Dyman, 2003). An increasing carbonate content trend is observed up section in the UEF which is related to a continued drop in sea level. Decreasing water depth during regression resulted in poorer TOC preservation than in the Lower Eagle Ford.

The AC was deposited in shallow oxygenated waters resulting in poorer TOC preservation (Pearson, 2012) and increased burrowing is also observed (Dravis, 1979). Proximal to the Maverick Basin, Harbor (2011) describes the bounding sections of the AC as highly cyclic laminated wackestone and a central section that is a bioturbated lime wackestone associated with a period of global eustatic high stand (Galloway, 2008) and bounding periods of relatively deeper water. The laminated sections suggest recurrent variations in water column oxygenation that produced sharp bounding contacts at the base of laminated facies. During this time the Western Interior Seaway remained connected to the GoM.

Volcanic activity began in Santonian when the upper Austin Chalk was deposited and continued through the Early Campanian. This activity was restricted to the Balcones Igneous Field, where an abundance of volcanic centers are found in Zavala County (Mathews, 1986). Explosive eruptions on the seafloor resulted in intense fracturing of the surrounding country rock (Ewing and Caran, 1982).

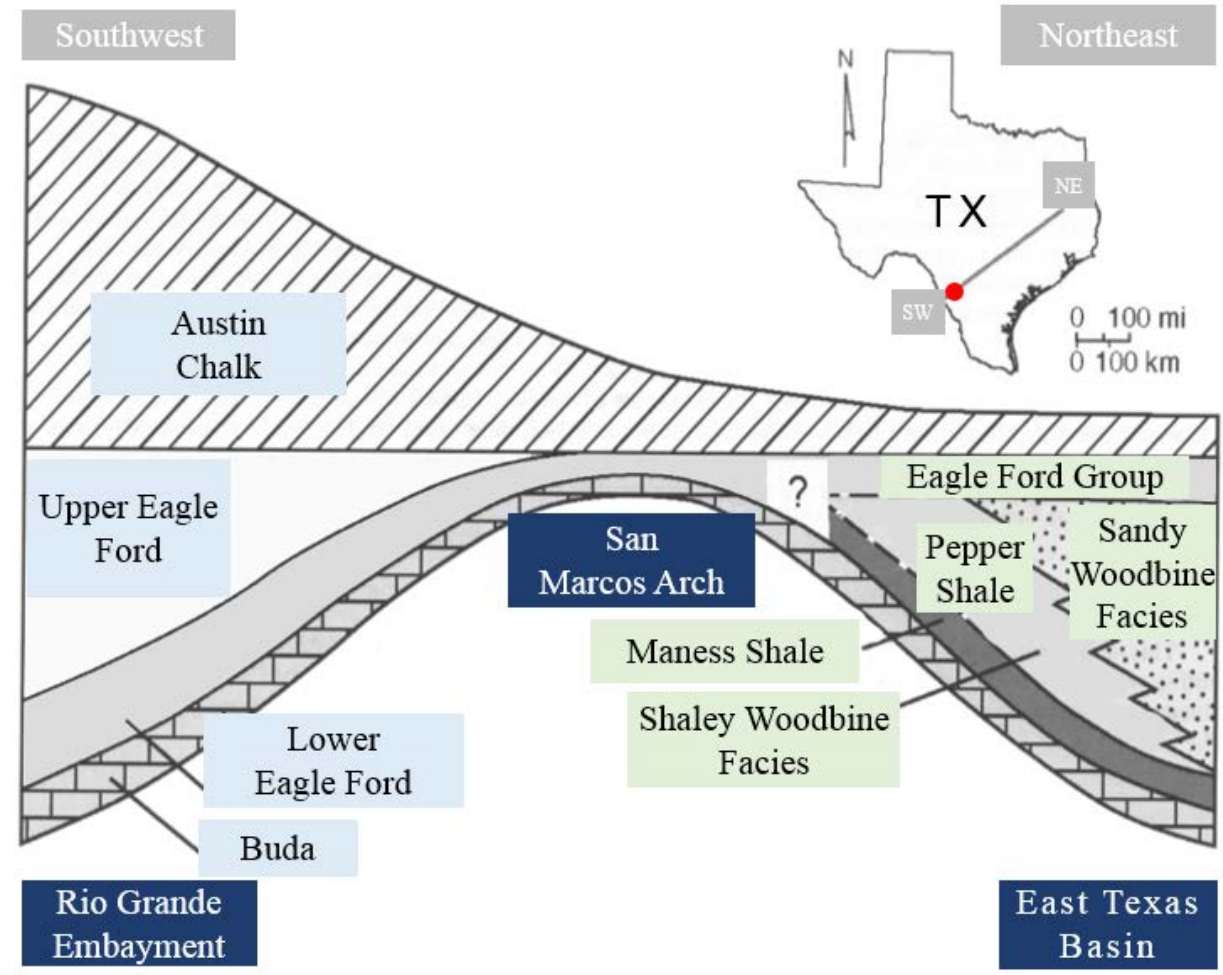

Figure 9. Schematic southwest to northeast cross section demonstrating the effect of the different depositional and structural settings through the Rio Grande Embayment, San Marcos Arch and the East Texas Basin, modified from Bennett, (2016).

Data Description

Stephens Production Company (SPC) provided access to a post stack 3D seismic volume processed through prestack time migration. The Pedernales survey is located about 75 miles southwest of San Antonio in Zavala County. Survey parameters are outlined in Table 1. Data from several wells were also made available by SPC, however only three were in the area of seismic coverage.

Table 1. Seismic parameters. The Dominant Frequency was calculated from 0.3 seconds above the top in the AC to 0.3 seconds below.

Seismic Survey		
Name	Pedernales	
Environment	Onshore	
Acquisition year	***2009***	
Area	40 miles^2 (approx.)	
Bin size	110 ft x 110 ft	
Sample rate	4 ms	
Reference Datum	Sea level	
Dominant Frequency	36.75 Hz	
	Austin Chalk	Eagle Ford
Avg. Interval Velocity	16,247 ft/s	14491.54 ft/s
Dominant Frequency	34.75 Hz	34.75 Hz
Vertical Resolution	111.29 ft	99.26 ft
Lateral Resolution	222.58 ft	198.52 ft

Table 2. Primary well log data used.

	Holdsworth Trust	**Holdsworth Nelson**	**Whitecotton**
Spud Date	03-17-2010	05-21-2010	12-05-1955
UWI	4250732752	4250732756	4250700160
KB (ft)	760	683	813
TVD (ft)	6496	6401	6709
Gamma Ray Logged (ft)	17-6434	20-6401	Na
Sonic Logged (ft)	2486-6407	2551-6348	Na
Density Logged (ft)	2486-6407	2551-6348	Na
Image Log (ft)	Na	4800-6000	Na

Table 3. List of all well and formation top information used. 1-6 were retrieved from DrillingInfo (2018), with 7-9 from Stephens. (Depths are in TVD SS.)

	API	Completion Date	KB	AC Top	EF Top	Status
1	4250732889	8/18/2012	677	4724	5356	Active
2	4250732891	8/12/2012	677	4729	5368	Active
3	4250732876	6/9/2012	700	4660	5300	Active
4	4250733071	12/29/2013	773	4932	5402	Active
5	4250732914	12/15/2012	680	4283	4915	Active
6	4250733202	1/30/2015	759	4849	5313	Active
7	4250700160	12/5/1955	813	4563	5117	Inactive
8	4250732752	4/16/2010	760	4630	5290	Inactive
9	4250732756	5/21/2010	667	4206	4883	Inactive

Methods

Seismic Interpretation

Seismic data is usually contaminated with both random and coherent noise even after the data has been migrated reasonably well and is multiple free (Chopra et al., 2011). Because seismic attributes are sensitive to noise (second derivative attributes such as curvature in particular) the Pedernales dataset was pre-conditioned before attribute calculation. Seismic attributes are useful for enhancing subtle geological features that are often hidden in the volume. Although there are hundreds of attributes formally recognized (Liner, 2016), only a handful will be utilized in this investigation.

A median filter was first applied to suppress random noise. Evidence exists that median filters are guilty of introducing high frequency noise that does not exist naturally in band limited data, particularly at data boundaries. However, this has not been observed in our data on the amplitude spectrum or by manual inspection of such boundaries.

Cretaceous horizons were tracked on the conditioned volume. Because the AC top is a discontinuous event that is heavily affected by the volcanics at the center of the seismic survey, a negative event at the base of the Anacacho was tracked and shifted down 24.5 ms by interpolation of the 4 ms time sample rate in to the place of the AC top. Weak, inconsistent event amplitudes due to small acoustic impedance contrast in the Austin Chalk interval resulted in no seismic events that could be tracked across the entire dataset in the AC. Events that could be tracked were converted to surfaces using a grid size of 110 x 110 for further interpretation.

The dataset was time-cropped between 600 and 1500 ms (TWT) centered on the AC interval to reduce attribute processing time. For subsequent discussion, this conditioned, cropped volume will be referred to as the Pedernales dataset. A Fourier amplitude spectrum was extracted from the Pedernales dataset with a dominant frequency of 34.75 Hz. Vertical and lateral resolution calculated for the AC is listed along with other data parameters in Table 1.

Volume Curvature

Curvature is a structural attribute that is used to delineate faults and predict fracture orientation and fracture density (Chopra and Marfurt, 2007a). Roberts (2001) describes in detail the algorithm, attributing positive values to anticlinal features, negative values to synclinal features and zero implies a planar surface with no curvature. Copra and Marfurt (2007b) state that the dip component of curvature is correlated to open fractures in central Texas, however Austin Chalk production has been documented from both open and closed fractures (Marfurt and Chopra, 2007a)

A high resolution dip model of the Pedernales dataset was calculated along both inline and crossline directions. This is necessary since estimates of dip reflector and azimuth of seismic time

cubes are only loosely related to the true dip and azimuth in depth (Chopra and Marfurt, 2007a). This high resolution model was then used to generate the curvature volumes.

Al-Dossary and Marfurt (2006) first introduced the concept of calculating curvature of different wavelengths, providing new perspectives of the same geology. Chopra and Marfurt (2011) describe how short wavelength (narrow aperture) curvature identifies highly localized fracture systems while long wavelengths enhance subtle flexures on the scale of 100-200 traces. For this investigation, a narrow aperture of 2x2 most positive and most negative curvature are included, although apertures of 5x5 and 9x9 were also examined.

Coherence (Variance)

Coherence is a geometric attribute that measures the similarity between adjacent traces that can be used to identify discontinuities (Bahorich and Farmer, 1995). Coherence (also known as variance) is sensitive to waveform changes that depend on lateral variability in lithology, porosity, density and fluid type. Variance can be used to extract subtle information regarding stratigraphy and structures that lie close to the resolution of the data. While fault visibility in the standard amplitude volume is sensitive to the relative strike of the fault, in the variance volume faults are equally visible regardless of their orientation relative to strike (Brown, 2011).

For this investigation a 2x2 filter is used for estimating horizontal variance. Vertical smoothening is used to enhance continuity in the volume, larger values (15+ samples) are typically used to reduce noise effectively but tends to smear edges detected in the volume. Because this thesis is focused on fractures (highly localized deformational features), a short filter size of 8 samples was used in variance computation to enhance these local discontinuities. Since the volume was already conditioned, areas that are highlighted with this technique are expected to be related to geology

and not an artificial result. It is also taken into consideration that Chopra and Marfurt (2007a) emphasize the importance of calculating variance in the dip direction for structural interpretation.

Ant Tracking

Ant tracking is an iterative scheme that attempts to connect adjacent zones that have been identified with previously run edge detection attributes pre-filtered to eliminate horizontal features associated with stratigraphy (Chopra and Marfurt, 2007a). It was first introduced be Pedersen (2001). Results are heavily dependent on signal processing and the edge detection attributes used in highlighting discontinuities.

Pedersen et al. (2002) describe the ant tracking algorithm in detail, referring to it as an 'enhanced attribute' capable of identifying features of sub-seismic resolution. The ant tracking workflow is divided into four steps

1) Seismic conditioning (I assume seismic conditioning is obvious to all geophysicists and needs no description here. A few general statements may be of use to us unenlightened geologists. Just a thought.
2) Edge detection; several attributes are useful for identifying discontinuities in the volume. Variance and curvature have been previously discussed. Chaos, a measure of the lack of organization in the dip and azimuth model, often used to enhance spatial discontinuities, is also commonly used in ant tracking. Different recipes of edge detection attributes have been discussed in ant tracking workflows. Fanghal and Zoback (2014) use variance as the sole edge detection input in their analysis of the Barnett Shale. Chopra and Marfurt (2007a) discusses the use of curvature, with the Petrel workflow also recommending chaos and dip deviation. Others have also used a combination of attributes including Fang et al., (2017)

in their analysis of a fractured carbonate reservoir in the Jingbei Oilfield, China. Ogiesoba and Klokov (2016) use most positive curvature as the fault attribute for their investigation of the Austin Chalk, so the same fault attribute will be used in this research

3) Application of ant tracking to highlight potential faults; the software allows the modification of 6 parameters to determine how these 'ants' will identify faults. These can be tailored to favor the identification of local events such as fractures or more regional features like faults. Baytok (2010) provides a detailed description of each of these parameters. Since local events are of interest in this study, an initial ant boundary of three voxels was selected. This defines the initial distribution of ants, whereby no ant will initially be placed within a radius of three voxels of another ant. Baytok (2010) recommends an initial distribution of three to four voxels for detailed mapping of small faults and fractures. Another critical parameter is the ant step size, defining the number of voxels the ant moves with each increment. By using a value of one, the resolution of the results increases, although limiting the area the ant can search. A full list of the parameters used are show in Table 4, with these parameters remaining consistent for each of the three separate ant tracking volumes generated. An additional stereonet tab is available that allows the restriction of the ants in specific dips and azimuths, this was not utilized.
4) Automatic Fault Extraction; was not used in this investigation.

Table 4: List of Ant tracking parameters used.

Initial Ant Boundary	Ant track deviation	Ant step size	Illegal steps allowed	Legal steps required	Stop criteria (%)
3	2	1	2	2	6

Depth Conversion

Depth conversion is the process of combining seismic time structure and well control to create a depth structure map or volume (Liner, 2016). The domain conversion is heavily dependent on the accuracy of the formation tops picked during the drilling of previous wells.

Using Schlumberger Petrel software an advanced velocity model was generated. A total of 9 wells (Table 2) were used in the depth conversion. At each well location a pseudo-velocity was calculated from the observed seismic travel time and the well formation top. These velocities were gridded to form a depth conversion velocity model. Surfaces of interest were then converted to the depth domain using this velocity model

Acoustic Impedance

Acoustic impedance (AI) is the product of density and P wave velocity and thus an interval lithological property, not an interface property like seismic data. As a result, seismic tuning (Liner, 2016) is diminished, resolution is increased and wavelet side lobes are removed, reducing the risk of false geological structures (Latimer et al., 2000). Strong empirical relationships between AI and rock properties such as lithology and porosity have been identified in the literature for both carbonate and clastic reservoirs. Brown (2011) offers a survey of different post stack inversion processes, along with their benefits and pitfalls, as well as a summary of inversion process.

For this project, Hampson Russell version 10 (HRS) was used since it allows the generation of several different inversion models in an all-encompassing 'Post Stack Inversion' workflow. Brown (2011) demonstrates that not all inversion algorithms are equally effective. Russell and Hampson (1991, p 877) state 'there is no absolute right way to do a post stack inversion'.

Latimer et al (2000) emphasises the importance of quality control of both the input seismic and well log data, as the quality of the final inversion is a direct result of the quality of the input data. Seismic data is band limited, with the highest and lowest frequencies absent as shown in Figure 10. The absence of higher frequency data is a fundamental limitation on seismic interpretation due to earth filtering effects, reducing the resolution of the data. Low frequencies are missing due to bandwidth limits on seismic sources and further loss by processing removal of noise. However, Pedersen-Tatalovic et al., (2008) emphasise the importance of this low frequency information. Targeting a chalk unit in the North Sea, they demonstrate the missing low frequencies caused their high impedance target to be masked. These results are echoed by Brown (2011) who states that for quantitative interpretation, these low frequencies are extremely important.

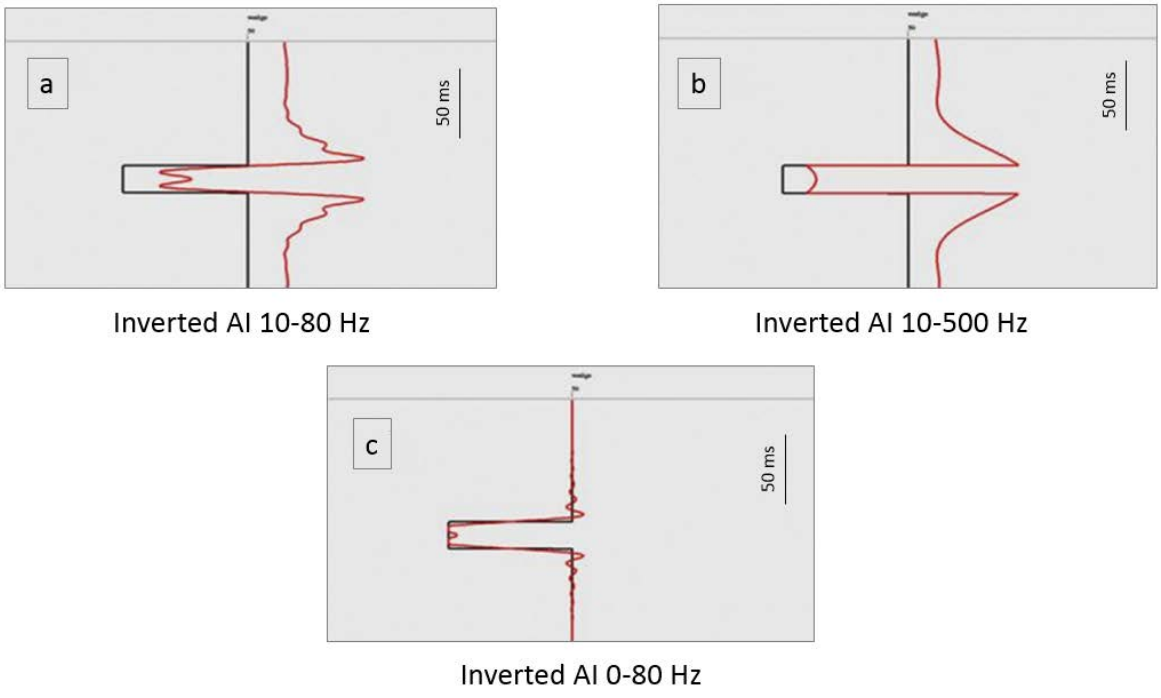

Figure 10. A simple impedance layer model inverted using three different frequency ranges. Inclusion of high frequencies allows better definition of the layer thickness but the inclusion of low frequencies allows absolute values to be recovered, taken from (Brown, 2011).

The Pedernales survey was imported along with the Holdsworth Trust and Holdsworth Nelson digital well logs, formation tops and tracked seismic horizons corresponding to those tops. Check shots were also imported and applied.

A synthetic seismogram is an essential part of the workflow. This process attempts to create a zero offset seismic trace that would have been theoretically recorded at the borehole (Liner, 2016), connecting the wireline logs with the seismic data. A poor tie can result in misinterpretation and poor quality results. Initially, an Ormsby wavelet set up to the corner frequencies of the data was used. A more accurate synthetic tie was achieved using a statistical wavelet extracted from a 3 x 3 radius around the well location over a time window of 600 ms centred on the Lower Austin Chalk. The use of a longer wavelet allows additional energy to be carried in the side lobes, with the use of a longer wavelet often necessary due to the presence of multiples in the data.

An initial model was generated that spanned the Pedernales survey. Sonic and density logs from the two wells record all units from the Anacacho to the top of the Buda, meaning that well log extrapolation is not necessary. With such limited well control, interpolation of values away from the well is a critical parameter. Inverse distance squared was determined to be the best choice of interpolation. No smoothening filter was applied to the modelled traces.

Five different post stack inversion algorithms are available in HRS; Band limited, Coloured Inversion, Model-Based, Sparse Spike Linear Programming and Sparse Spike Maximum Likelihood. Previous seismic investigations into the AC were assessed to determine which method of inversion would be best suited. Results of pre-stack inversions and inversions of refraction data dominate the literature so the search was expanded to include seismic investigations of the underlying EF. Kumar et al (2014) and Chen et al. (2015) compare results from a coloured and

model-based inversion used to predict porosity in the Lower EF in south west Texas. Based on these earlier studies, three different inversion models will be investigated.

1) *Bandlimited*; also referred to as a recursive inversion (Russell, 1988) and a relative inversion (Brown, 2011) in the literature, is the oldest and simplest inversion algorithm. It is based on the convolutional model of the seismic trace (Lindseth, 1979):

$$S = W * R + N$$

Where S is the seismic trace, W is the wavelet, R is the reflection coefficient series (or reflectivity) and N is noise, which is assumed to be random in the Pedernales dataset as a result of prior conditioning. Reflectivity is the contrast in acoustic impedance (often denoted Z) between two interfaces. The inversion process involves rearranging of this relationship to give:

$$Z_{i+1} = Z_i \left(\frac{1+R_i}{1-R_i}\right) \quad (1)$$

Russell and Hampson (1991) note that the exact reflectivity will not be recovered due to noise, residual wavelet and amplitude problems, with the inversion producing only an approximation. Because it is based purely on reflectivity, it will exhibit the same frequency bandwidth as seen in the post stack seismic data, meaning frequencies higher and lower than the source bandwidth will be absent. Brown (2011) describes how the lowest frequencies, from the low end of the seismic band (2-10 Hz) down to 0 Hz, can be incorporated into the impedance inversion from well log data. This gives a more accurate result as impedance values are scaled to rock values, however it is cautioned that artefacts and large impedance errors can result from incorrect well interpolation and recovery of very low frequencies (0-2 Hz). HRS uses a constraint high cut frequency parameter to

recover missing low frequency data from the wireline data. Based on the amplitude spectrum, an 11 Hz cut off frequency was used.

2) *Coloured Inversion;* similar to a recursive inversion, with Lancaster and Whitecombe (2000) describing the algorithm as not necessarily the most accurate, but it is fast and ideal for preliminary investigations. An unconstrained sparse spike inversion is modelled as a convolutional process, with an operator whose amplitude spectrum maps the mean seismic spectrum to the mean earth AI spectrum, and has a phase of -90°. Because this operator is convolved directly on the seismic data, traditionally this method has been band-limited. In modern software it is possible to add in the lower frequency, which was not in the current investigation because Chen et al. (2015) chose not to add low frequencies in their assessment of the Lower EF. Assumptions of this method include zero phase input data and reflectivity spectra from the wells representative of the true reflectivity in the survey area, which may not always be true (Brown, 2011).

3) *Model-based Inversion*; often referred to as blocky or layered inversion, involves building an initial geologic model and comparing the results to the seismic data, with the results of the comparison used to iteratively update the model in such a way as to better match the seismic (Russell, 1988). This has many advantages, including a greater frequency spectrum and it avoids inverting the seismic data directly. However, the problem of non-uniqueness arises as it is possible to have a model that matches the seismic very well but is incorrect. This can be limited by a good understanding of the geology. For the current project, a generalized linear inversion in HRS is used to accomplish model-based inversion. This eliminates the need for trial and error by analysing the error between the model output and then perturbing the model parameters in such a way as to produce an output with less error

(Russell, 1988). Here, the problem of non-uniqueness can be limited, by the use of constrained model rather than a stochastic model which simply merges the traces with the initial geologic model. The constraint model allows both hard and soft constraints to be utilized with respect to how far parameters can deviate from the initial model, with hard constraints applied.

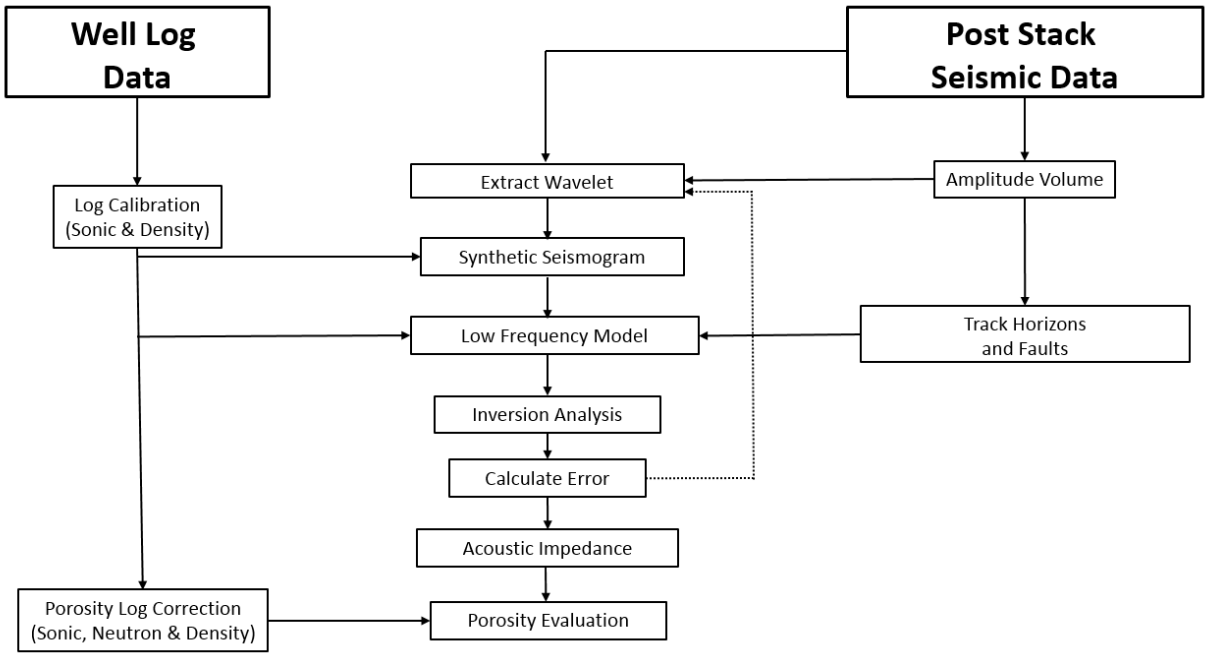

Figure 11. Workflow for the Model-based Inversion, see text for discussion.

Well Log Methods

Formation tops called by drillers typically list informal subdivions of the Austin Chalk (AC). Traditionally the letters A through E were assigned, with E referring to the basal AC in the Pearsall Field. However, these sub units are not clearly defined in the literature or within the survey and are not used. Instead, the AC is subdivided into three lithological units -- termed Upper, Middle and Lower -- based on the gamma ray (GR) curve. A middle, cleaner carbonate lies between upper

and lower interbedded shale and carbonate units. Three porosity logs (sonic, neutron and density) were available for both the Holdworth Nelson and Holdsworth Trust, all calculated against a carbonate matrix.

Three kinds of porosity are distinguished and related to well log measurements.

1. The sonic log yields matrix (primary) porosity. The sonic tool measures the interval transit time of compressional waves travelling through the formation. Sonic porosity is dependent on lithology since the Wylie time-average equation (Wylie, 1958) requires a matrix interval transit time:

$$\emptyset_S = \frac{t_{log} - t_{ma}}{t_f - t_{ma}} \quad (1)$$

Where:

$\emptyset_S$ = *sonic (matrix, primary) porosity*

t_{log} = *interval transit time from the log reading*

t_{ma} = *interval transit time of the matrix (limestone = 47.6 μs/ft)*

t_f = *interval transit time of the formation fluid (189 μs/ft)*

Sonic porosities calculated using the Wylie equation in carbonates fail to record porosity associated with fractures or vugs, and as a result are used as an analogue for matrix porosity (Asquith and Kygowski, 2004).

2. Total porosity is measured using density and neutron porosity. The density logging tool emits Gamma Rays from a radioactive source which collide with electrons in the formation losing energy to Compton scattering predominantly. High energy returning GR is related to electron density which is turn proportional to the bulk density of the formation (Tittman

and Wahl, 1965). The formation bulk density is a function of matrix density, formation fluid density and porosity and is calculated using;

$$\emptyset_D = \frac{\rho_B - \rho_{ma}}{\rho_{ma} - \rho_f} \quad (2)$$

Where:

$\emptyset_D$ = *density porosity*

ρ_B = *formation bulk density (log reading)*

ρ_{ma} = *matrix density (limestone = 2.71 g/cm^3)*

ρ_f = *interval transit time of the formation fluid (1.1 g/cm^3)*

The neutron log measures hydrogen concentration. As a result it can be influenced by the presence of clay and/or shale since the neutron log responds to hydrogen concentration and shales contain clays that have substantial amounts of absorbed, or bound, water. To overcome these effects, a neutron-density (ND) log was created using,

$$\emptyset_{ND} = \left(\frac{\emptyset_N{}^2 + \emptyset_D{}^2}{2}\right)^{1/2} \quad (3)$$

Where:

$\emptyset_{ND}$ = *neutron-density porosity*

$\emptyset_N$ = *neutron porosity*

$\emptyset_D$ = *density porosity*

3. Secondary (fracture, vuggy) porosity is identified in carbonates by subtracting matrix from total porosity (Asquith and Kygowski, 2004). The percentage of secondary porosity, commonly referred to as the Secondary Porosity Index (SPI), is the focus of this study. It is not possible to determine if local increases in secondary porosity are associated with

fractures or vugs on wireline data. However, an image log is available for the Holdsworth Nelson well and is consulted for further evaluation.

Results

Seismic Interpretation

Cretaceous horizons tracked in the Pedernales survey were converted to surfaces. The Austin Chalk (AC) top (UAC) and base (LAC) are included in Figure 12. Both surfaces show a definitive dip towards the south east. The AC top shows structural features with two volcanic mounds clearly visible and a third existing immediately to the west, at the perimeter of the survey. No volcanic features are seen on the AC base as is expected, however depressions are observed lying directly beneath the volcanic mounds that are attributed to velocity draw down.

Faulting is visible on the AC top, but not the base. This is similar to what is presented in the geoseismic section in Figure5. Faulting is evident and abundant in the overlying Anacacho Limestone and UAC, however it appears to die out with depth in the Middle to Upper AC. No clear fault offset identified using the standard amplitude volume was observed in the LAC.

The UAC and LAC surfaces were converted to the depth domain for further inspection. Formation tops from 9 wells were used for the domain conversion. Two of the most southern wells are situated very near one another and as a result only 8 well tops are visible on the velocity maps. From the distribution of wells, a more accurate conversion is expected in the south of the survey where the well density is higher.

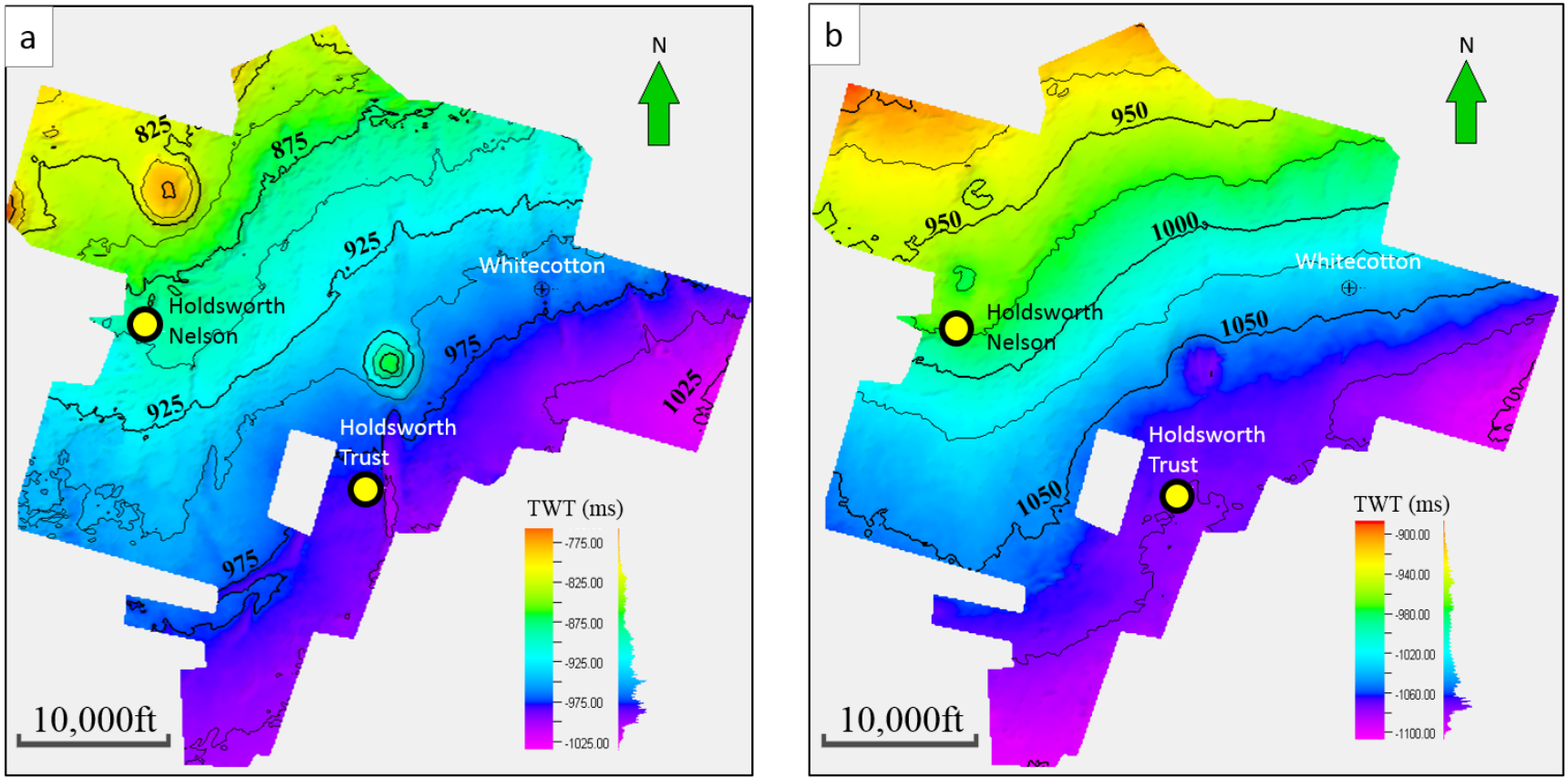

Figure 12. Austin Chalk (a) Top and (b) Base time structure maps, with the primary wells used in the investigation also annotated. Both maps demonstrate a dip to the southeast. Volcanic mounds and faults are prevalent on the AC top map while no faulting is seen on the AC base. Contour interval: 25 ms.

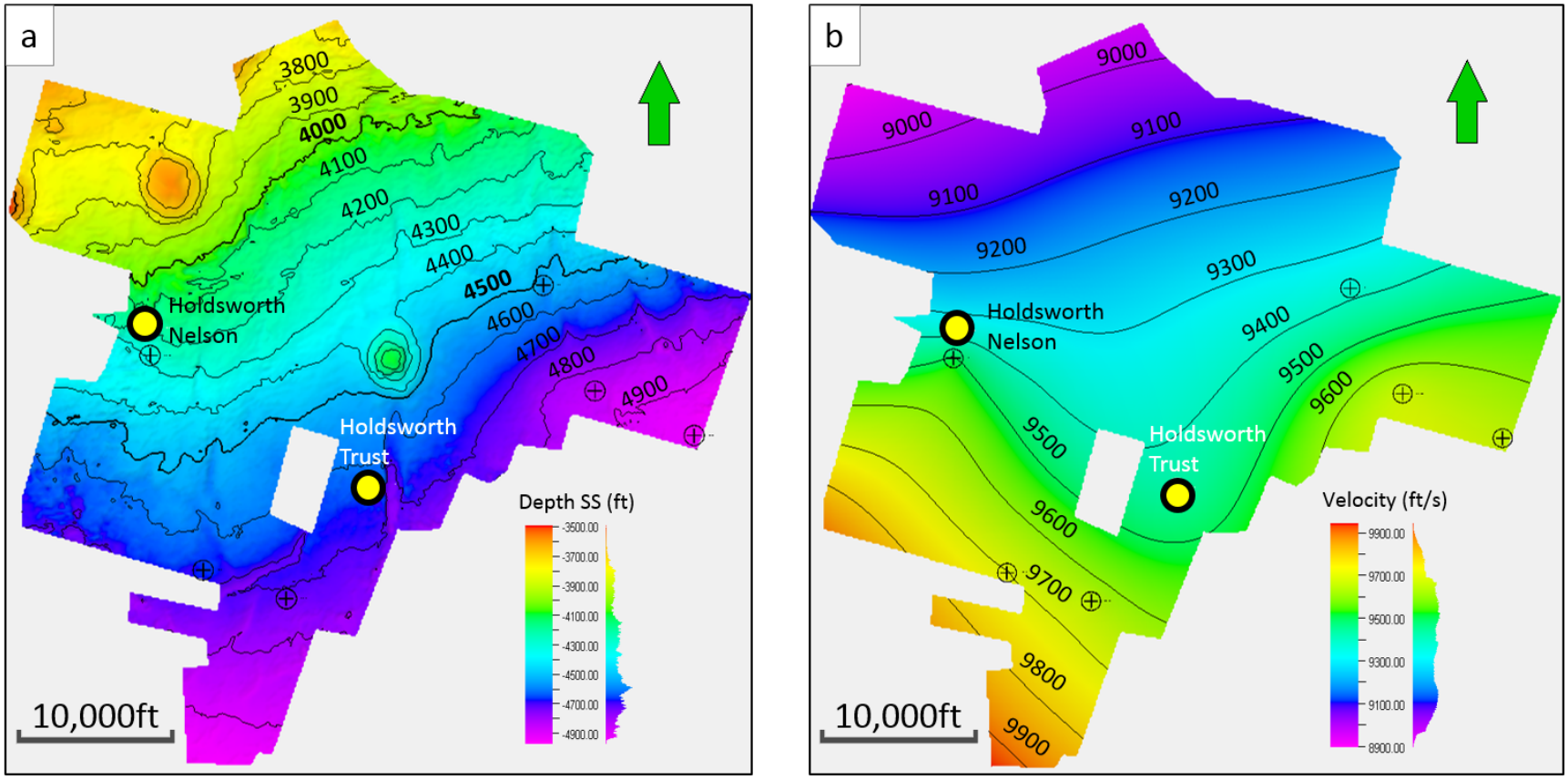

Figure 13. (a) Austin Chalk top depth structure map in ft subsea with control from 9 wells. Again volcanic mounds and faults are visible on the AC top. (b) The average velocity from the AC top to sea level. Trend of increasing average velocity towards the southeast.

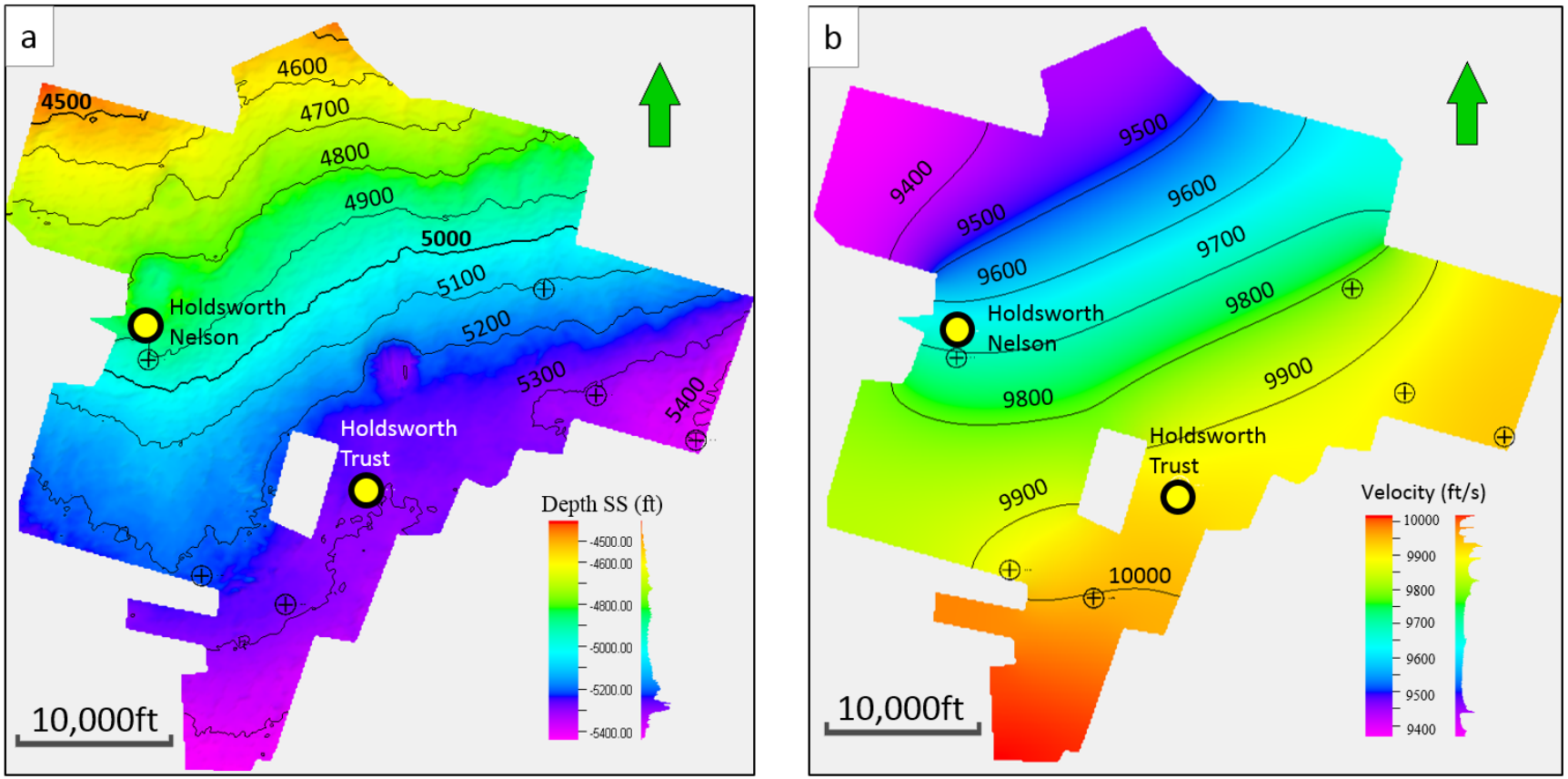

Figure 14. (a) Eagle Ford top depth structure map, with no clear faults disrupting contours. Depths are displayed in ft subsea and a clear trend of increasing dip towards the southeast with an average dip of close to 2 degrees. (b) Average velocity map of the Eagle Ford top and sea level, generated with control from 9 wells.

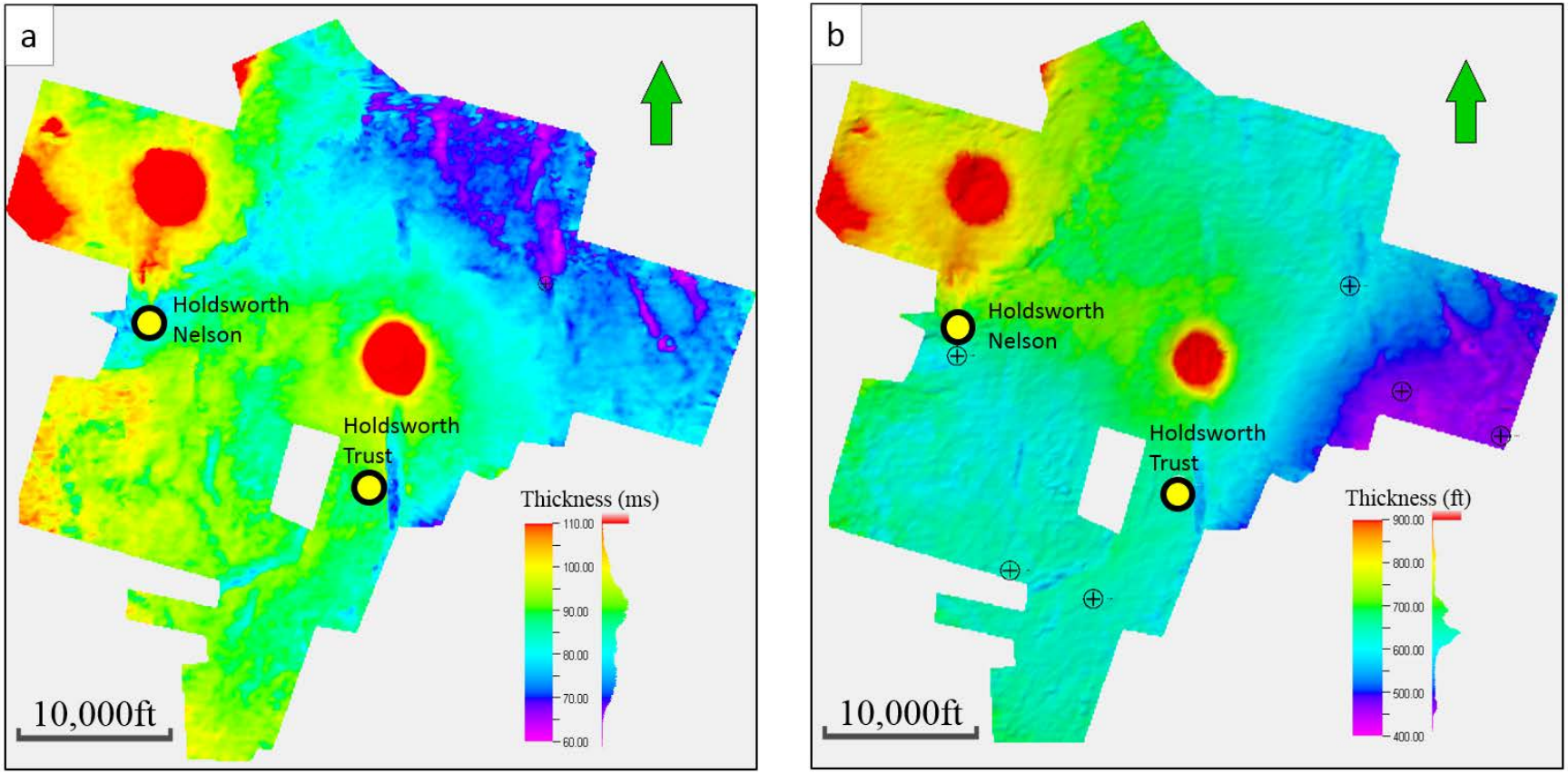

Figure 15 Austin Chalk thickness map in (a) time and (b) depth. Both maps emphasize the greater thickness of the volcanic mounds within the survey. Different behavior can be observed between the central volcanic mound and the mounds in the northwest on both maps. Faults are highlighted in these thickness maps, however closer inspection shows that these are seen in the Upper AC, not the Lower AC. Both maps show similar trends besides the northeast corner, however this is attributed to poor well control in the northern half of the survey.

An isopach map is also produced between the UAC and top Eagle Ford depth surfaces, showing the absolute thickness of the AC (Figure 15). Areas included within the volcanic mound show significantly increased thickness. This is partly attributed to the submarine volcanic mounds being structurally positive features on the surface of the Upper AC. However, volcanic material in the Uvalde Volcanic Field shows an interval velocity of close to 11400 ft/s (Ogiesoba and Eastwood, 2013), much lower than the interval velocity of the Lower AC observed in well logs within the survey (15750-16500 ft/s). Due to the significant difference in velocity, two-way time sag is expected to cause significant amplification of thickness of the AC in the area immediate to the volcanic mounds. Because no well data is available for the volcanic mounds within the survey and since the mounds are not the focus of this investigation, the thickness in these areas is not corrected.

Long linear trends of reduced thickness are seen on the isopach map that correlate with faults visible on the surface of the AC Top. These trends are largely striking N25E, N60E or N40W. On closer inspection, these isolated areas of reduced thickness show that faults penetrating the UAC appear to die out or significantly reduce their offset below the resolvable limits of the data in the Lower AC.

For all seismic attributes, a 20 ms time window above the Eagle Ford Top surface was extracted to capture the effects of vertical to sub-vertical faulting in the Lower Austin Chalk. The effects of acquisition footprint were investigated by examining time slices of the shallowest amplitude volume; no evidence of amplitude banding parallel to acquisition direction was observed. Thus the features described in the following sections are assumed to be geologic in origin rather than due to acquisition footprint or other seismic noise.

Variance

Variance (Bahorich and Farmer, 1995) was applied to identify deformational structures in the Lower AC (Figure 16). High variance is observed in the northwest corner of the survey; however, this is understood to be an edge effect of the survey perimeter or migration fringe (Liner, 2016). Such adversely high and low magnitude responses are seen on other maps in the same location and will not be investigated.

Several areas of high variance are identified away from the migration fringe. An area of high variance is identified near the central volcanic mound. This is very distinctive with values rising as high as 0.45. Areas of more subtle variance are also apparent. About 500 ft southwest of the Holdsworth Trust well, two subtle linear features are seen almost parallel to one another, with values reaching as high as 0.15, striking approx. N25E (green). Similar magnitudes and orientations are seen in other parts of the surface. Because of their low value and distinct shape, it is most likely that these features are faults, but they have offsets below the resolvable limits of the data.

An area of high variance is also observed near the Holdsworth Nelson well. This area of increased variance is slightly elongated, almost unorthodox in shape. Although this feature lies close to the edge of the surface, this response initially did not appear to be an edge effect as is seen to the north. The absence of such high variance responses to the south and orientation of the west flank of the Pedernales survey, leading to the conclusion that the Pedernales survey was most likely cut from a larger survey for interpretation and these responses were geologic in nature.

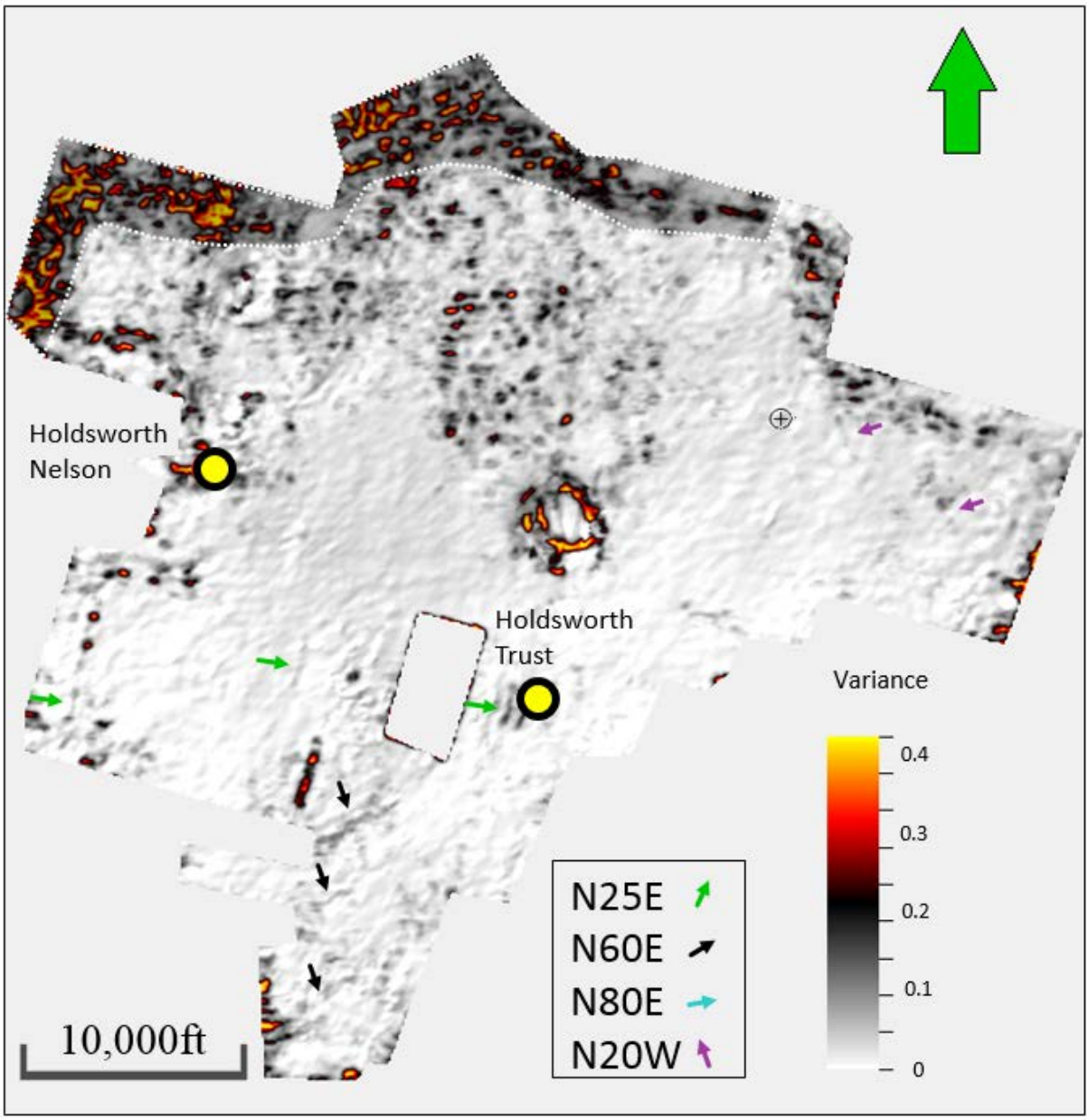

Figure 16 Variance map of the Lower AC, calculated using a 2x2 filter length, over a 20 ms up window. High values in the northwest (highlighted), are attributed to edge effects and are not geological features. Arrows are used to label some of the trends identified.

Volume Curvature

Most positive and most negative curvature (Chopra and Marfurt, 2011) results are overlaid with one another to delineate faulted and folded zones. Far more features are highlighted in Figure 17 than the variance map previously discussed. Trends orientated N60E and N80 become apparent.

Overlap of the most positive and most negative curvature is observed in the north west of the survey. These overlap areas produce a red colour that is very distinctive and suggests an error of some sort since most positive and most negative curvature respond to separate geologic features. This is seen in the area affected by the migration fringe in the northwest but also near the Holdsworth Nelson well. This unorthodox feature seen on the variance map, appears in red in the curvature display, and as a result is most likely not a geologic feature and will not be investigated any further.

The N25E trend identified near the Holdsworth Trust well is more prevalent on the curvature display, particularly in the southwest of the survey. Beginning in the south of the survey, there is a very prominent trend of features highlighted striking approx. N60E (black). While the variance map subtly delineated one such feature, the curvature map shows this trend much more distinctly.

Ogiesoba and Eastwood (2013) applied most positive curvature to their Austin Chalk base horizon, also tracked on a PSTM volume with a time sample rate of 2ms in Dimmit County (30 miles south of the Pedernales survey). Faults delineated on the base of the Austin Chalk in Dimmit County were all consistently striking north eastward with two dominant trends; N28E-N31E and N51E. Significantly larger faults were associated with volcanic mounds. The majority of these faults identified on the base of the AC appear as fold bends, as opposed to faults, in seismic amplitude data despite a 2 ms time sample rate.

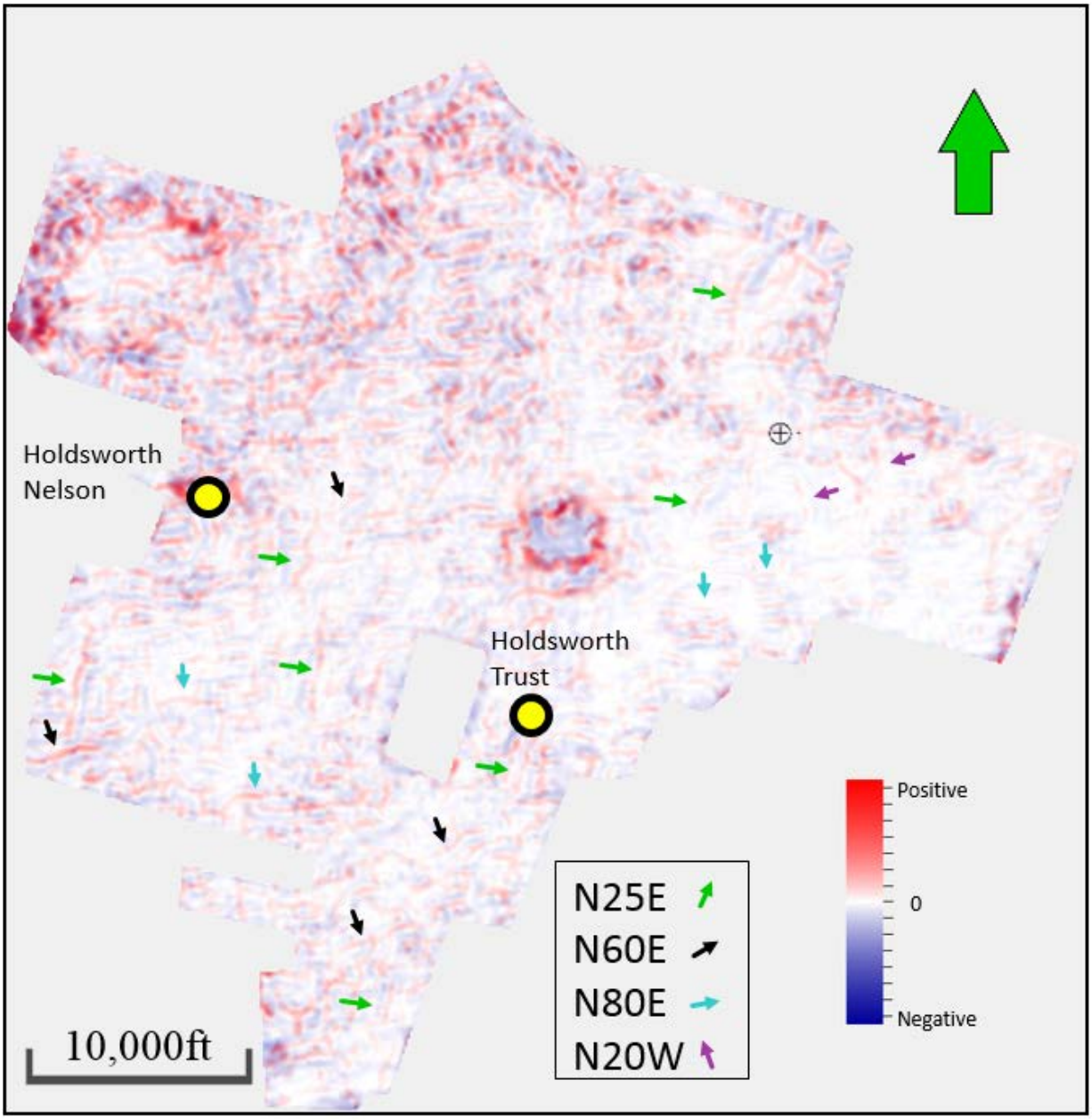

Figure 17. Most Positive and Most Negative curvature of the Lower AC overlaid. Curvature was calculated on a short (2x2) wavelength. Most positive values suggest an anticlinal features, while most negative values suggest a synclinal features (Roberts, 2003). Overlap of most positive and most negative results are seen in some areas. Since these curvature attributes respond to two different geological features, it is most likely that these results are not geologic in nature. Arrows are used to label some of the trends identified.

Ogiesoba and Eastwood (2013) applied most positive curvature to their Austin Chalk base horizon, also tracked on a PSTM volume with a time sample rate of 2ms in Dimmit County (30 miles south of the Pedernales survey). Faults delineated on the base of the Austin Chalk in Dimmit County were all consistently striking north eastward with two dominant trends; N28E-N31E and N51E. Significantly larger faults were associated with volcanic mounds. The majority of these faults identified on the base of the AC appear as fold bends, as opposed to faults, in seismic amplitude data despite a 2 ms time sample rate.

Consistent trends identified by variance and curvature in the Pedernales survey strike N25E and N60E, conforming to those results observed to the south in Dimmit County. Although Ogiesoba and Eastwood (2013) did identify these features, they did not speculate the cause of these two different fault orientations observed. A subtle yet noticeable trend striking approximately N80E (teal) is also seen in the south of the Pedernales survey on the curvature display. A N20W trend is also visible.

Ant Tracking

In addition to variance and curvature, a more detailed fault identification attribute, ant tracking (Pedersen, et al., 2002), was also applied (Figure 18). Ant tracking has been shown to identify sub seismic resolution features in unconventional reservoirs including the Marcellus Shale. Wilson et *al.* (2014) interpreted small faults and fracture zones based on the ant track output in the Lower Marcellus Shale that were not identified with other attributes. The fault attribute utilized for pre-processing was most positive curvature. This shows far more features than identified on both the previous attributes, although results are not entirely consistent with the previous attributes.

The relatively round shape of the central volcanic mound can be identified, with the north western volcanic mound less discernible. The migration fringe which produced adverse results in the north western corner of the variance and curvature maps does not appear to produce such adverse responses. Ant tracking also shows the subtle N20W orientation that curvature highlighted, however with greater distribution.

The orientations of faults are much more chaotic, due in part to the volume of features identified, this is expected due to ant tracking being a more detailed attribute. The N80E faulting trend is much more prevalent and with greater distribution on the ant tracking surface than either of the two other fault attribute maps. While curvature showed quite low magnitude values relative to the other orientations observed on the previous attributes, the N80E trend shows the highest magnitude responses on the ant tracking display.

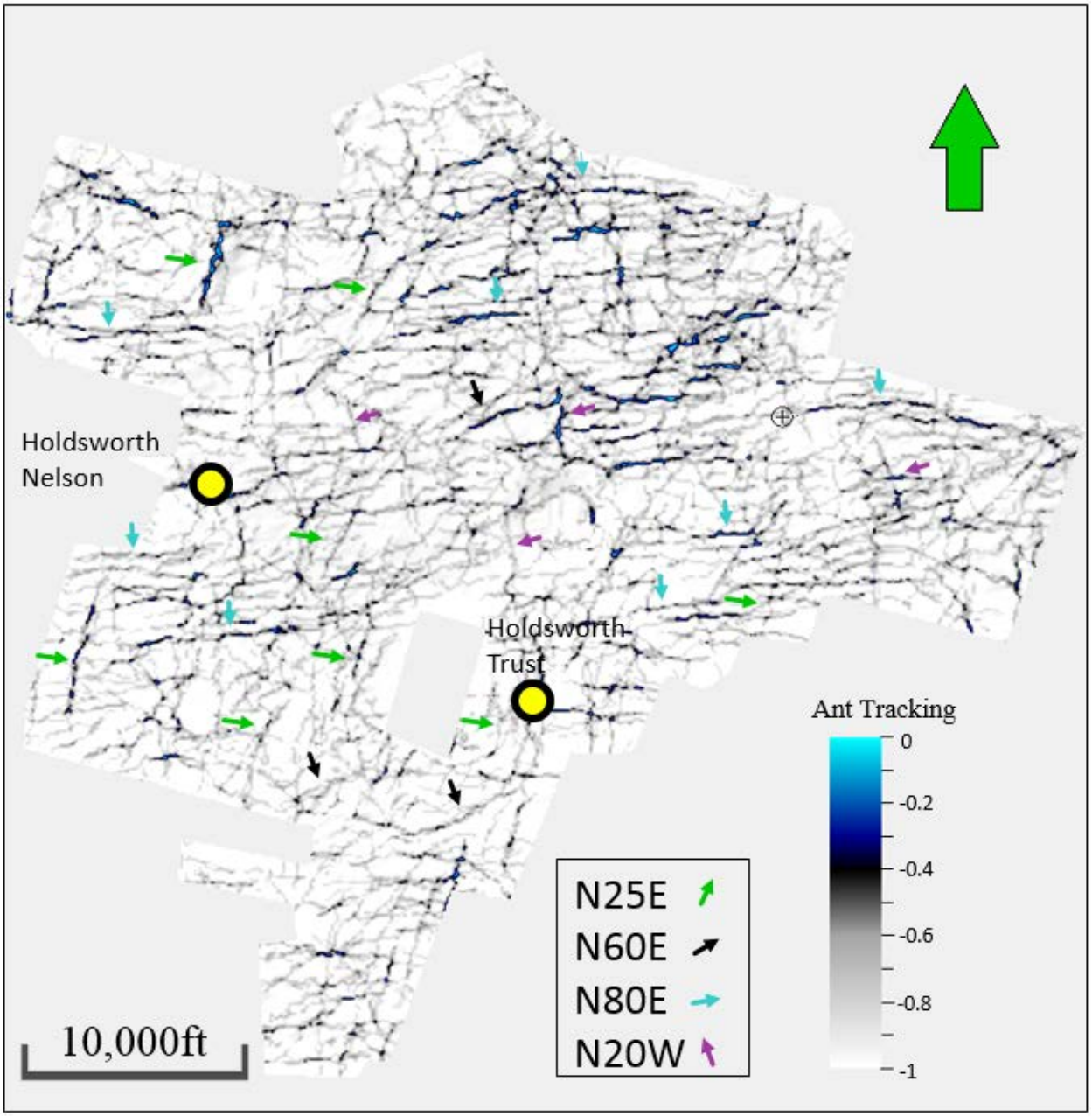

Figure 18. Ant tracking results of the Lower Austin Chalk using parameter displayed in Table 3. Arrows are used to label some of the trends identified.

Seismic Post Stack Impedance Inversion

Post stack impedance inversions have been used in several investigations targeting the Austin Chalk (e.g. Ogiesoba and Eastwood, 2013; Clemons et al., 2016) and Eagle Ford (Chen et al., 2015). Good to excellent relationships between wireline properties and AI have been observed in carbonate and unconventional reservoirs including the Austin Chalk. By upscaling well log properties though a calibrated AI volume areas of interest can be identified and investigated. Secondary porosity in conjunction with discontinuity attributes are used to investigate for potential fracture swarms.

Three different inversion methods were applied to the Pedernales survey using two wells for control. Model-based inversion was shown to be the most accurate with the lowest error (Table 5). Despite the proximity of the Holdworth Nelson well to the edge of the Pedernales survey, higher correlation and lower error is observed for all inversion methods.

Table 5: Results of the different seismic inversion methods. Correlation refers to the synthetic trace with the field trace.

	Holdsworth Nelson		**Holdsworth Trust**		**Average**	
	Correlation (%)	Error (ft/s*g/cm3)	Correlation (%)	Error (ft/s*g/cm3)	Correlation (%)	Error (ft/s*g/cm3)
Coloured	75.15	1799.9	63.37	2085.3	69.26	1942.6
Band Limited	82.21	741.7	78.02	1506.6	80.115	1124.15
Model-based	95.76	936.4	92.28	1256.7	94.02	1096.55

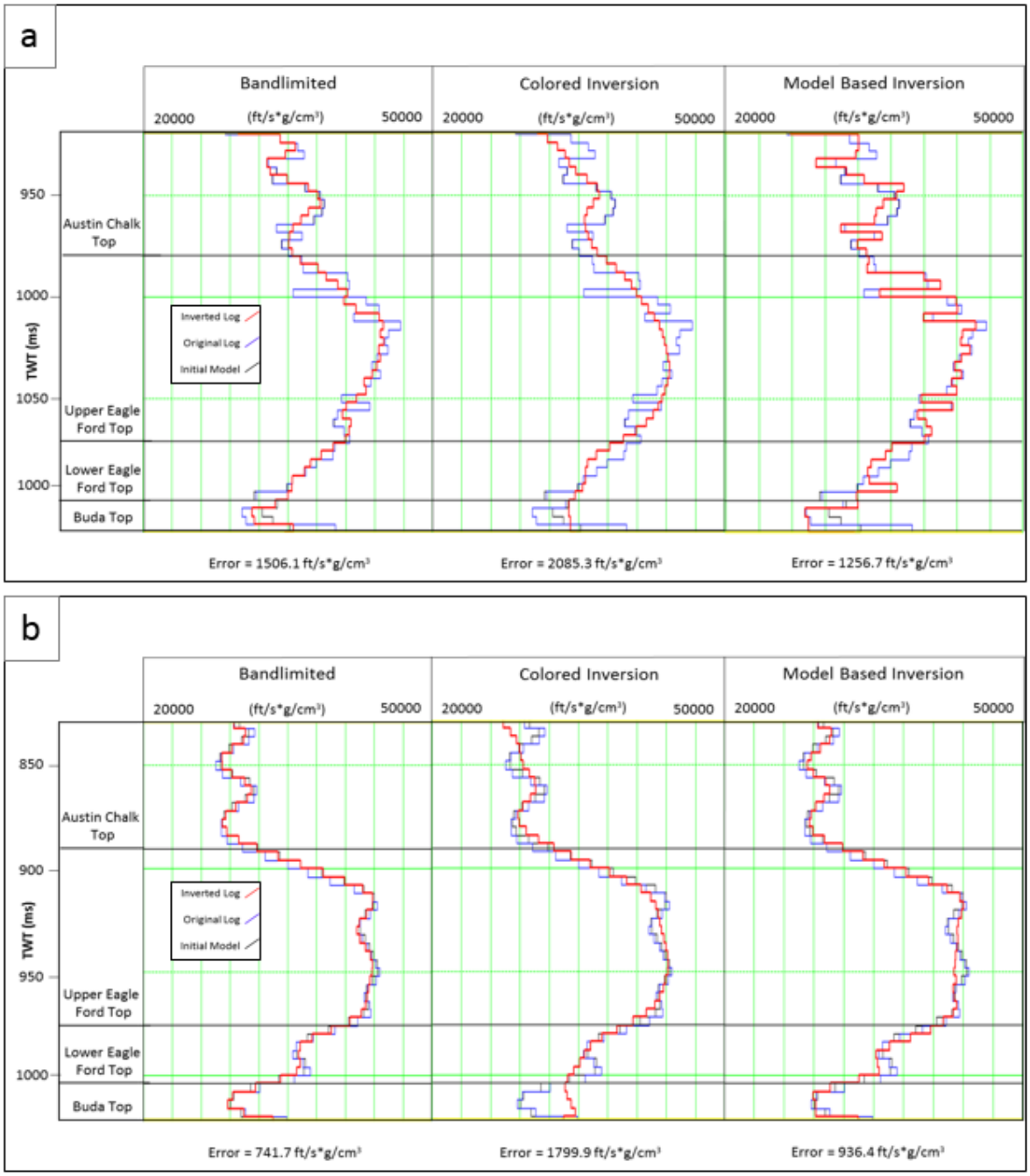

Figure 19. Comparison of different inversion methods used on the Pedernales dataset for the (a) Holdsworth Trust and (b) Holdsworth Nelson wells, between the Anacacho Top and the Lower Eagle Ford. Error and correlation accuracy are summarized in Table 5.

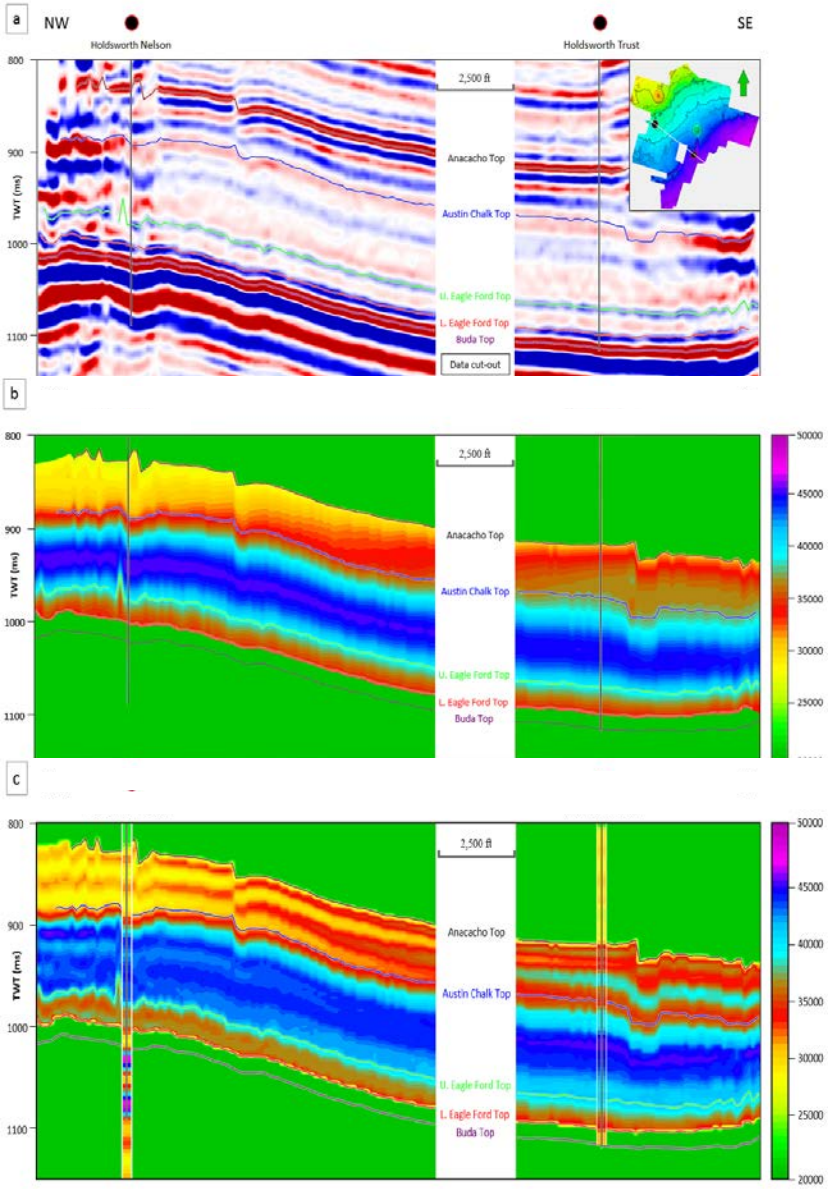

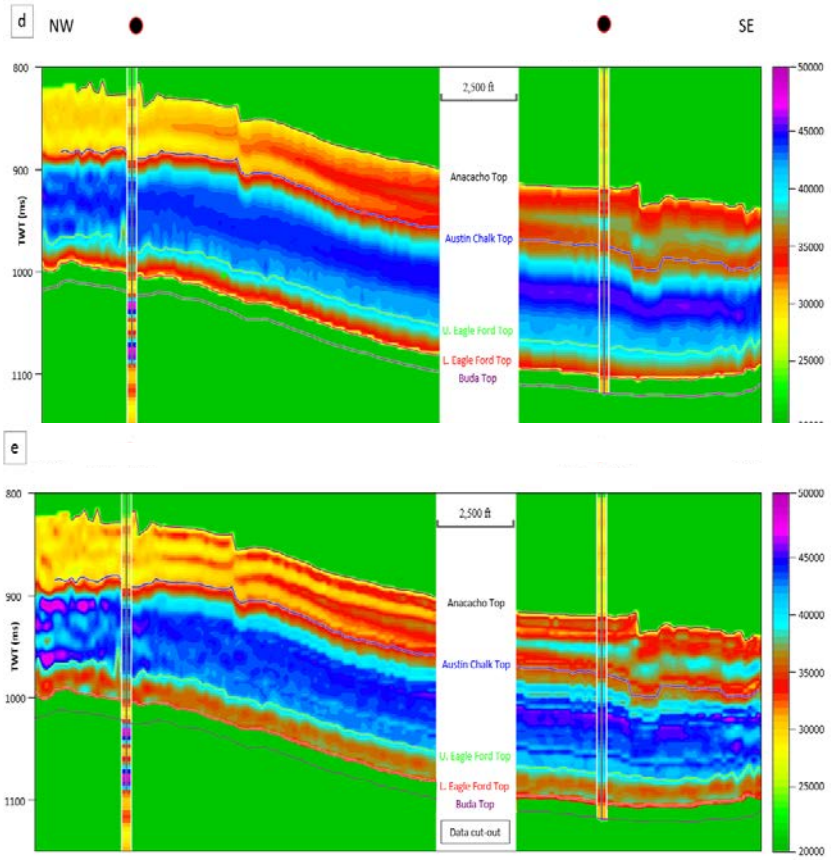

Figure 20a-e provides a visual comparison between the (a) amplitude volume, (b)Low Frequency Model (c) Band Limited (d) Colored and (e) Model-based Inversion. See text for further discussion.

Figure 20 (a) shows an arbitrary line, through the seismic amplitude volume, between the two wells used in the inversion. All Cretaceous units exhibit a dip towards the southeast, however the angle of dip is not consistent across the survey. Faults with clear offset are visible in the overlying Olmos (not labelled) and the Anacacho Limestone. 750 ft and 3000 ft southeast of the Holdsworth Nelson and 1000 and 1800 ft west of the Holdsworth Trust well such faulting occurs. Fault offset appears to terminate in the Middle AC, with interpretation hindered by poorer amplitude constraint than the overlying and underlying units. The Lower AC Base appears as a continuous reflector in Figure 20 (a) with no clear faulting, although the reflector does demonstrate subtle folding near the Holdsworth Nelson well.

Below the Austin Chalk, several longer wavelength folded features are visible in the Buda and older Cretaceous units near the Holdsworth Nelson well. These lie below faults in shallower units such as the Anacacho Limestone. Smirnov (2018) has shown that these faults are down thrown to the northwest, opposite to that of the overlying units. This behaviour was also reported by Ogiesoba and Eastwood (2013) in Dimmit County.

A high amplitude response is visible in the very northwest of the Lower Austin Chalk. This is the same area where the unusually shaped high variance response near the Holdsworth Nelson well was identified.

Figure 20 (b) shows the acoustic impedance (AI) low frequency model (LFM) generated in Hampson-Russell when applied to the interval between the Anacacho Top and the Lower Eagle Ford Top. This volume is comprised solely of data extracted from Holdsworth Nelson and Holdsworth Trust well logs. Highest values are seen in the Middle Austin Chalk in the NW where values reach up to 46000 ft/s*g/cm^3. The LFM shows a consistent trend of decreasing AI with depth below the middle AC as far as the top of the Lower Eagle Ford.

Figure 20 (c) shows a cross section of the Band limited AI inversion result. The wireline AI is displayed at the well bore for visual comparison with the surrounding AI volume, indicating a good correlation. This band limited inversion recovered the low frequency data using the LFM. Far more detail is presented within the AC interval than available in Figure 20 (b). A much more variable AC base is seen in the bandlimited inversion, with higher AI (44500 ft/s*g/cm^3) observed in the NW and gradually transitioning to lower AI values (40500 ft/s*g/cm^3) in the southeast.

Figure 20 (d) the coloured AI inversion also recovered low frequency data. Again the wireline AI is displayed at the well bore. For the Holdsworth Trust there is good correlation between the wireline and AI volume. However at the Holdworth Nelson wellbore, poorer correlation is observed in the Upper Austin Chalk and the Upper Eagle Ford. Again, a very general trend of decreasing AI from northwest to southeast is observed. Several features of interest appear between the Holdsworth Nelson and the data cut-out in the Lower AC along the cross section. Here local pockets of increased AI are seen that lie directly above subtle folds on the AC base.

Figure 20 (e) the AI results prove the model-based inversion to be the most accurate. Again a general trend is seen in the Lower AC of decreasing AI towards the southeast with AI values of up to 50000 ft/s*g/cm^3 noted at the most northwest edge of the cross section. This corresponds to the high amplitude area seen in Figure 20 (a). A good visual fit between the wireline AI and AI volume is seen, which is expected based on the results in Figure 20 and Table 5. In the area between the data cut-out and Holdsworth Nelson well, just like Figure 20 (d), there are increases in AI, although not as localized and closely related to subtle folds on the Lower AC surface.

To evaluate the AI inversion, a surface was extracted from the model-based inversion volume along the Austin Chalk Base over a time window of 20 ms up, to remain consistent with the fault attributes surfaces extracted.

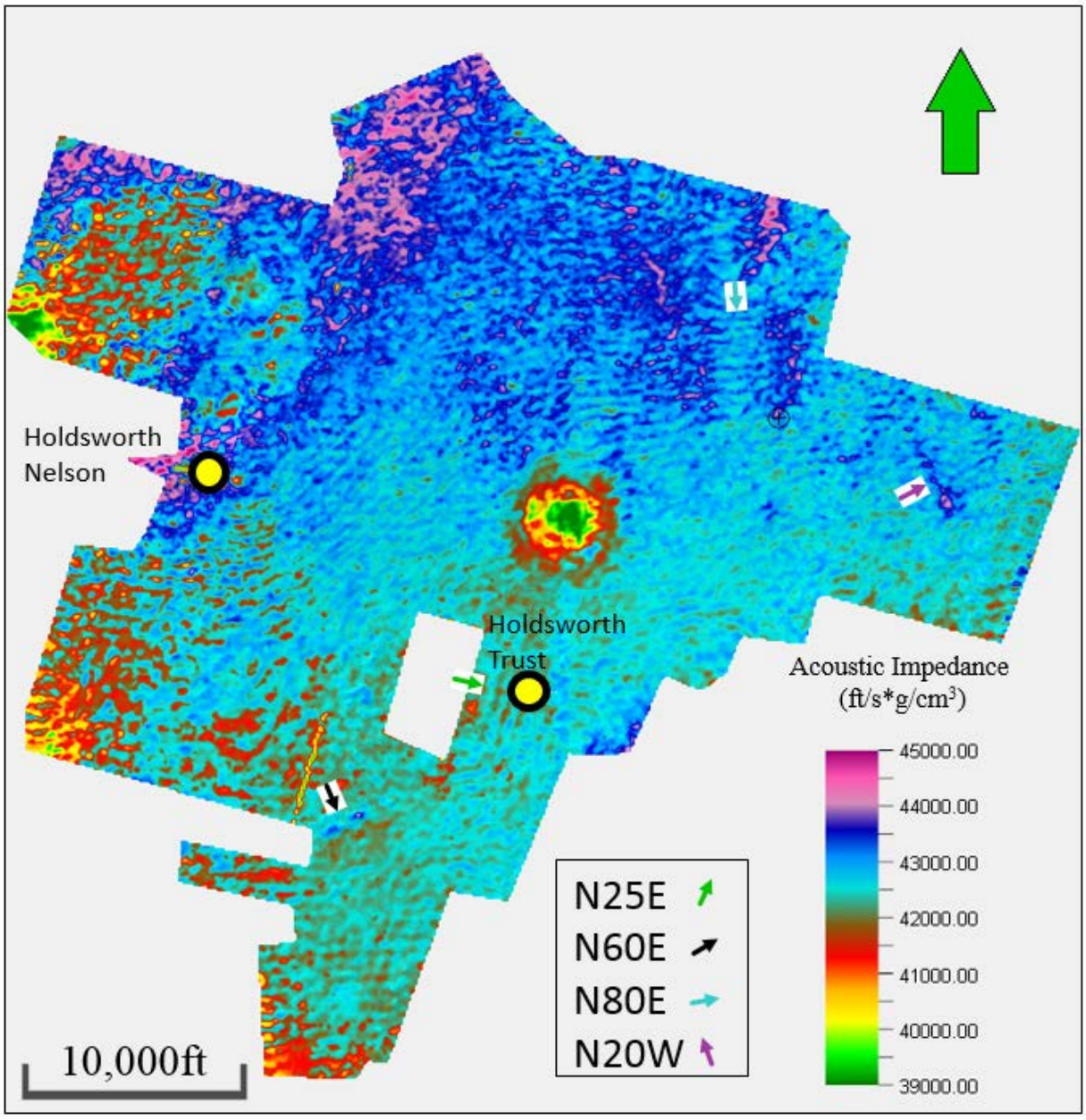

Figure 21. Model-based AI of the Lower Austin Chalk extracted over a 20 ms up window. Extremely low values are associated with volcanics and larger values with brittle rocks. Similar orientations are observed to those on the attribute maps, some of which are labelled. White dotted line highlights anomaly around the Holdsworth Nelson well.

Extreme high and low AI values are seen in the northwest corner of the survey. Like the variance map, these responses are again believed to be artifacts related to the migration fringe.

The central volcanic mound shows drastically lower values than the surrounding country rock. Values drop below 39000 ft/s*g/cm^3 in the center of the mound, with a surrounding halo like feature with an average value of 40750 ft/s*g/cm^3. Outside of the 3000 ft diameter of the mound, the country rock distinctly rises to more regular values. Lower AI is also observed in the northwest volcanic mound, with values dropping as low as 41250 ft/s*g/cm^3. This mound is overshadowed by the much larger, migration fringe influenced, low AI zone to the west. Ogiesoba and Eastwood (2013) also encountered lower AI within volcanic mounds in Dimmit County.

Several distinct elongations are observed on the Lower Austin Chalk AI surface, following similar orientations to those identified by the fault attributes. Both distinct and gradual transitions in AI are also seen. An area of high AI up to 45000 ft/s*g/cm^3 is seen immediately to the west of the Holdsworth Nelson well, encompassing a central, elongated low AI zone.

Well Log Analysis

Sonic, neutron and density logs from the Holdsworth Nelson and Holdsworth Trust and a fullbore formation micro-imager (FMI) log from the Holdsworth Trust were the main logs used in this investigation. Much of the well log analysis was carried out in Schlumberger Techlog. The Austin Chalk (AC) was first divided into three lithological zones using the gamma ray (GR) curve, where the Lower AC was characterized as a cyclical unit, lying below a middle clean carbonate unit. It is possible to further subdivide the Lower AC into units less than 50 ft thick on the GR curves of both wells, however these units would lie significantly below the resolution of the seismic data. Both the Holdsworth Trust and Holdsworth Nelson show consistent caliper readings throughout the Lower AC.

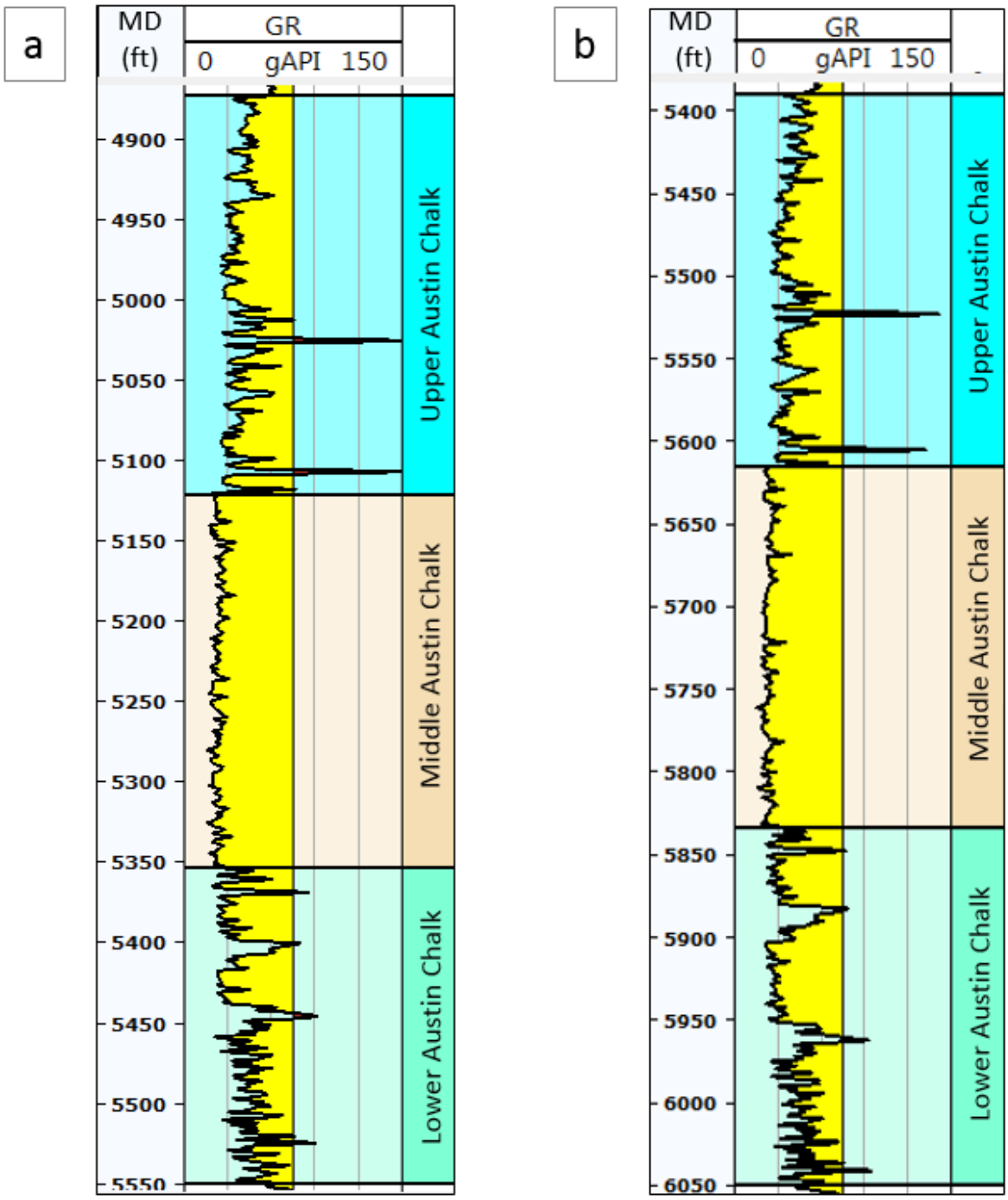

Figure 22. Gamma Ray log of the (a) Holdsworth Nelson and (b) Holdsworth Trust divided into upper, middle and lower units. Subunits of the Lower Austin Chalk can be seen that are below resolution.

Corrected sonic porosity (a proxy for matrix porosity) and neutron-density porosity (a proxy for total porosity) were cross plotted for the Lower AC interval in both wells (Figure 23). Both the Holdsworth Nelson and Holdsworth Trust data points lie above the equity line, indicating that secondary porosity is present in both wells (Asquith and Krygowski, 2004). Although this does not distinguish vuggy from fracture porosity, consultation of the FMI log will be used to classify secondary porosity type.

The FMI log was previously interpreted and could not be further digitally evaluated as it is a pdf file. The results of the FMI, included in Track 6 of Figure 24, are used to classify secondary porosity. Faulting and fracturing on the FMI log is indicated in a 30 ft bench near 5440 ft MD, with the rest of the borehole showing no fractures. Secondary porosity is highlighted in Track 5 of Figure 24 in red and is classified based on the result of Track 6. Secondary porosity is attributed to fractures in the 30 ft deformed bench and attributed to vug development in the rest of the Lower AC. Vuggy porosity rises as high as 4% near the base of the Austin Chalk while in shallower areas, is seen to drop to almost 0%. Secondary porosity values average 1.2% with a high of just under 3% within the secondary bench. Secondary porosity is attributed to fracture development with no vugs seen on the FMI.

This fractured bench correlates with a spike in the PE curve. (Track 4, Figure 24). Values outside of the fractured bench generally sit in the 4-5 range which is typical for standard carbonate lithologies and agrees with observations made by Martinez-Torres (2002) in the Giddings Field. Values in the area of bench at 5440md rise as high as 6. Crain (2010) points out that a PE value greater than 5 can be used as a fracture indicator when barite-containing mud is used. Barite has a PE value of 267 barns/electron, thereby the PE curve should demonstrate a very sharp peak in a

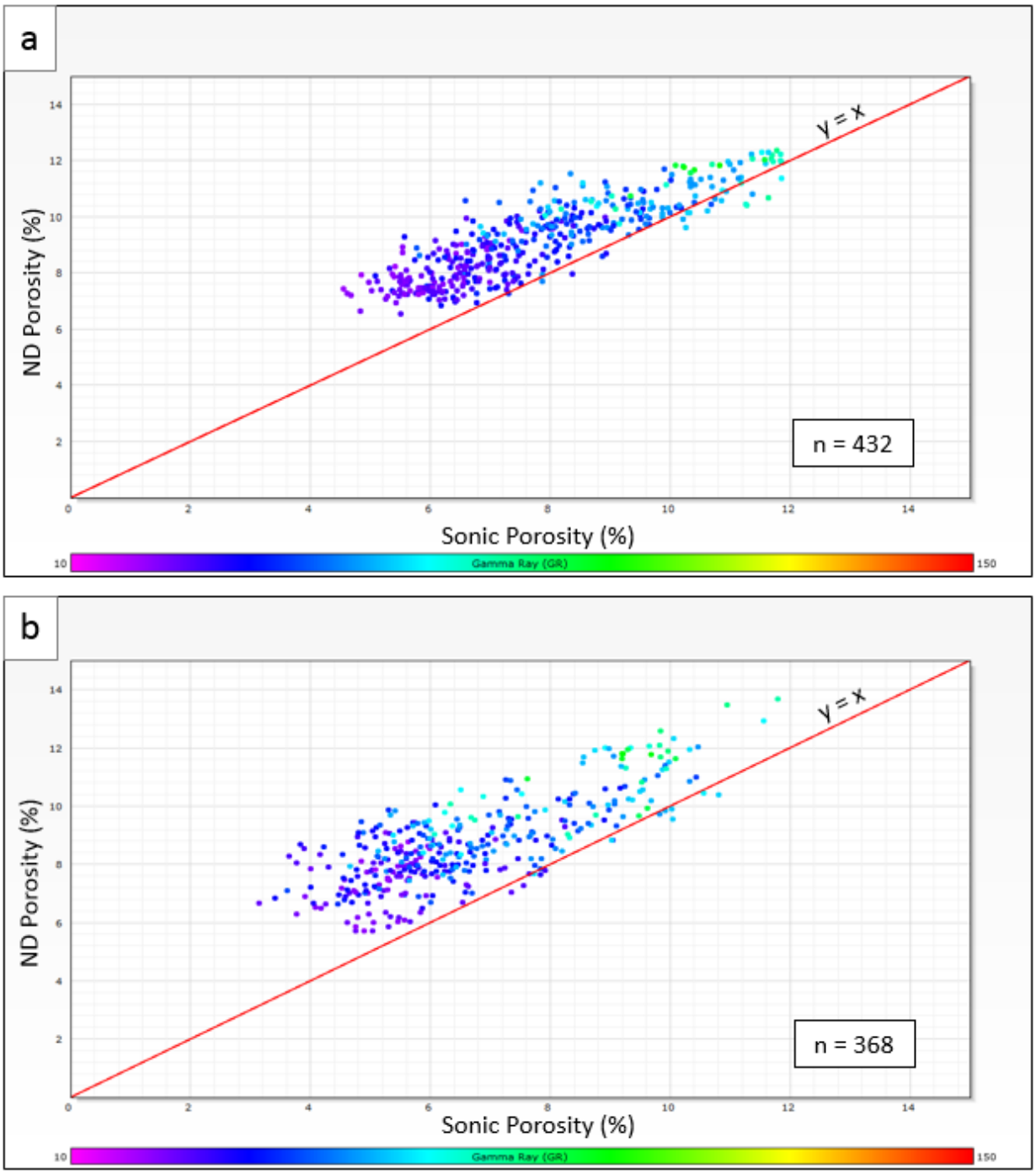

Figure 23. Cross plot of corrected sonic and neutron-density porosity for the (a) Holdsworth Trust and (b) Holdsworth Nelson. Data is expected to plot above the equity line since neutron-density measures total porosity and sonic porosity measures matrix porosity. Deviation above the equity line can be explained by the presence of secondary porosity.

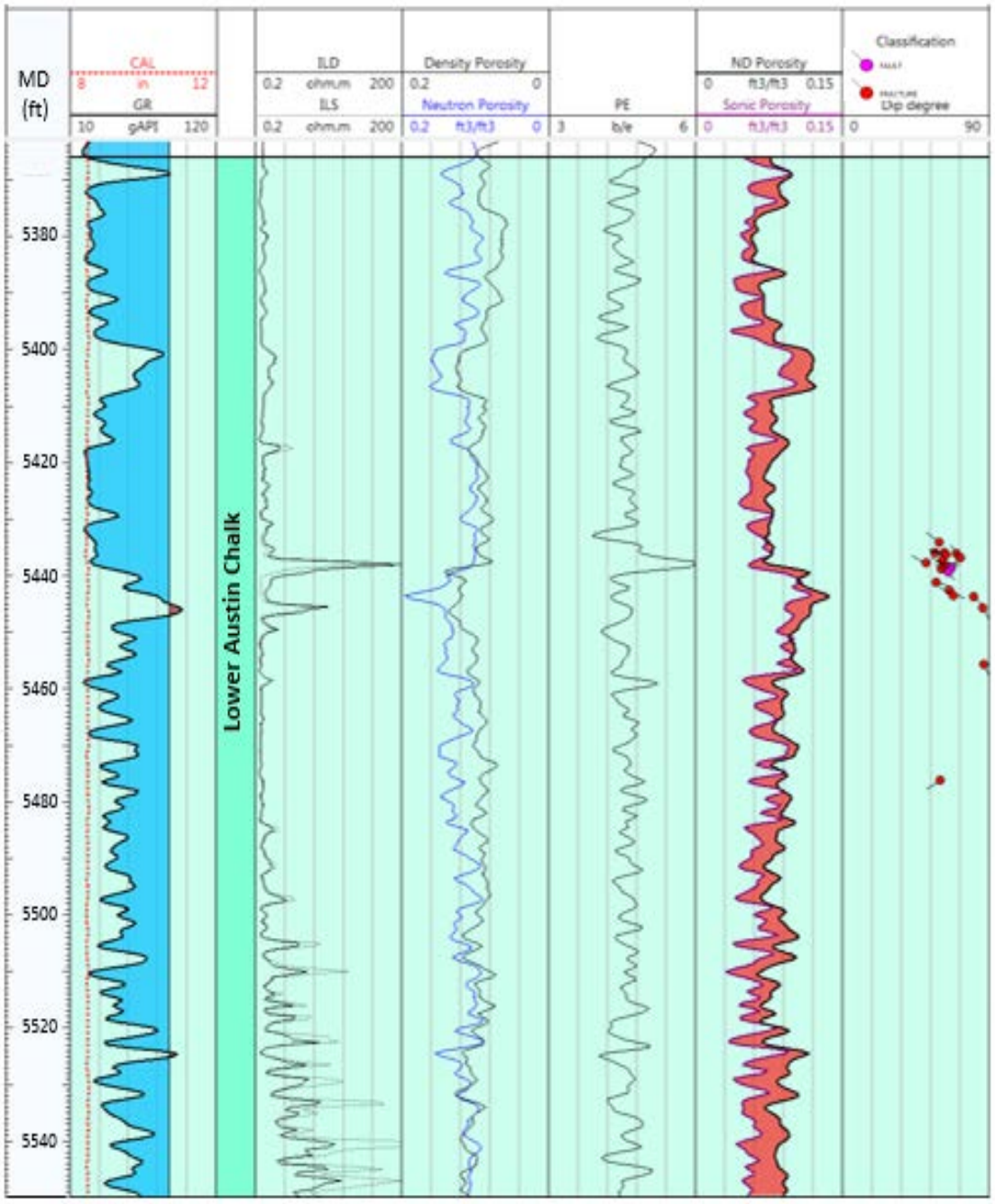

Figure 24. Well log display of the Lower Austin Chalk in the Holdsworth Nelson. See text for discussion.

fracture filled with barite loaded mud. The PE spike shows very good correlation with the FMI results.

Outside of the fractured bench, variation in PE values are a result of the variations in carbonate and shale material encountered. The PE curve is more detailed than the GR (Asquith and Krygowski, 2004), since GR is averaged over 2 ft and PE is not. As a result, more cyclicity is seen in the PE curve. Values closer to 5 contain almost pure calcite, while decreasing values represent a greater shale presence (Asquith and Krygowski, 2004). An increase in density porosity (Track 3, Figure 24) implies a drop in total density within the fractured bench. There is minimal crossover of the density and neutron porosity log suggesting some gas presence (Asquith and Krygowski, 2004).

Two spikes on the resistivity curve of the fractured bench are observed, 200 and 25 Ohms, with a 5ft interval between these spikes where the deep induction (ILD) log is greater than the shallow induction (ILS) log. Near the base of the unit, cyclicity is also seen in both the ILS and ILD, however the magnitude of cyclicity in ILS is far greater.

The AI volume was calibrated for total and matrix porosity using the regression equation from the wireline data (Figure 25). The matrix volume was then subtracted from the total porosity volume, producing a secondary porosity volume. A surface from each of these three volumes was extracted along the base of the Austin Chalk over a 20 ms up window to allow comparison with the seismic surfaces (Figure 26).

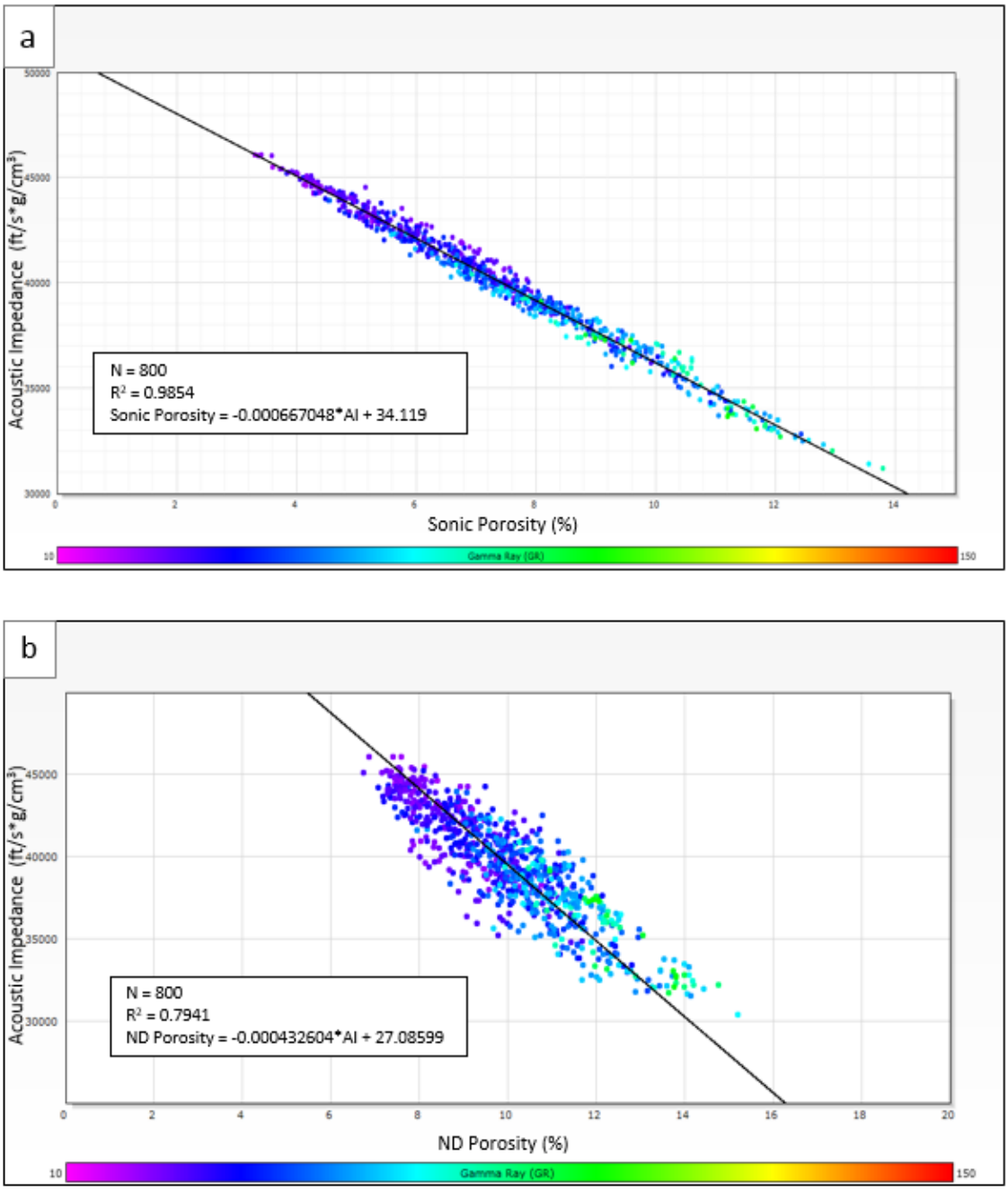

Figure 25. Shows the linear relationship between AI and (a) sonic porosity and (b) Neutron-density porosity used to calibrate the AI volume. Well data from the Holdworth Nelson and Holdsworth Trust is combined for each of the graphs, showing good consistency between the wells. Increasing secondary porosity is seen with increasing AI values.

Porosity Maps

Austin Chalk total porosity (Figure 26 (a)) varies between 7.5 and 10%. The highest total porosity is seen in the center of the volcanic mound, with another area of high porosity seen to the far west of the survey also associated with volcanics. In general, the northern half of the survey shows lower total porosity than the southern half, which is slightly counter intuitive. Subtle trends of increased porosity are seen in all areas of the map, most of which are linear.

Austin Chalk matrix porosity (Figure 26 (b) in general shows greater values in the south of the survey than in the north. This is counter intuitive since Dravis (1979) concludes that matrix porosity in the AC decreases with increasing depth, and depth increases to the south in the Pedernales survey area. Greatest matrix porosity values are also seen in the volcanic mounds.

Austin Chalk secondary porosity is typically attributed to either fracture or vug development. The volcanic mounds show minimal secondary porosity which is discussed later. Several linear trends are observed (Figure 26 c) in a variety of orientations. The largest secondary porosity observed is 2% which is seen on the downthrown side of a fault. Fracture porosity is essential for increasing permeability in the tight carbonate unit and allows communication and production of hydrocarbons stored in the matrix pore space. Adding 2% pore volume by fracturing to a rock with 8% matrix porosity, increases hydrocarbons in place by 25% and brings total porosity to 10%. Permeability is also vastly increased although difficult to quantify. Snyder and Craft (1977) describe fracture porosities of 0.1-0.25% as common throughout the Austin Chalk which significantly increases permeability in the Pearsall Field.

Ewing and Caran (1982) produced a schematic model of an erupting submarine volcano in the Upper Austin Chalk and Anacacho Limestone for the nearby Travis Volcanic Field. They note

intense ‘fracturing by explosion’ in the area surrounding the magma chamber that occurs because of the eruptions. While it is possible that such fracturing could be healed post eruption, no such increased secondary porosity was detected in the Lower Austin Chalk associated with the volcanic mounds. In fact, the area directly underneath the volcanic mound shows secondary porosity values of less than 1%, some of the lowest values found on Figure 26 (c), with values increasing with distance from the center of the mound.

Ogiesoba and Eastwood (2013) note that the magma feeders in the Uvalde Volcanic Field are often not found directly beneath these mounds and can be instead seen up to one mile away. Even with this increased search radius, no ‘fractures by explosion’ could be identified. Although there is a distinct linear trend seen directly to the south of the volcanic mound, this is associated with a tectonic fault with offset seen in units as young as the Olmos.

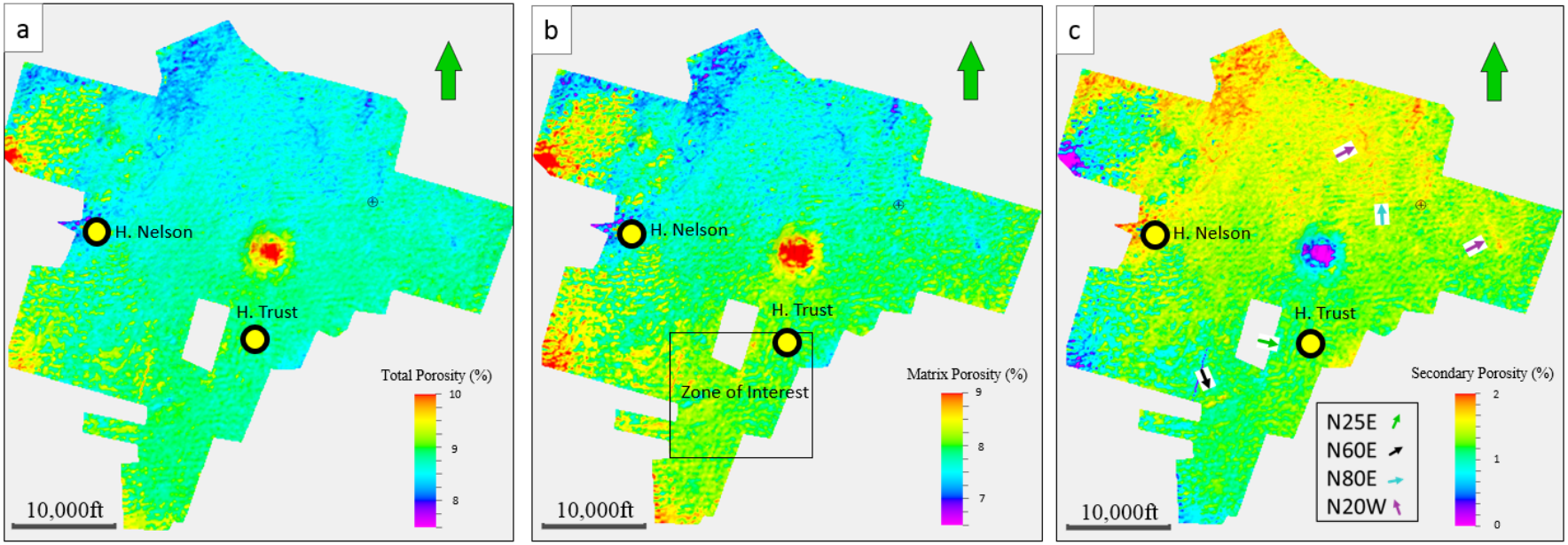

Figure 26. Porosity maps of the Lower Austin Chalk calibrated using relationships identified with the wireline data. (a) Total porosity was calibrated using the neutron-density log. (b) Matrix porosity was calibrated using the sonic log, (c) Sonic porosity was calculated by subtracting the matrix from total porosity volume and is attributed to fracture and/or vuggy development. Some of these subtle linear trends have been annotated on Figure 26 (c).

Area of Interest

This section of the survey includes the data cut-out previously denoted in Figure 19 and a minor, linear data cut-out not previously mentioned, visible on the very west of Figures 26.

Figure 26 (a), shows the variance map, highlighting two trends; one striking approx. N25E and the second striking N60E. Two features are seen striking N25E with a magnitude of 0.15 and running parallel to one another; these are located less than 500 ft southwest of the Holdsworth Trust well. Variance does not indicate whether the downthrown block is to the east or west.

The second features on Figure 26 (a) highlight a discontinuity in the seismic data striking N60E. Again, from variance it is not clear whether drop down is to the northwest or the south east.

Figure 26 (b) shows a blend of most positive curvature and most negative curvature, depicting more features than the variance map. In Zone A, a structure is again observed with orientation N25E, however based on the way the two curvature surfaces align, it appears that only one structure is present. In Zone B, a feature striking N60E is seen, consistent with that of the variance map. Both the N25E and N60E trend are more distinct in the curvature display. Based on the curvature display, the N25E trend shows drop down to the west, while the N25E trend shows drop down to the southeast.

Figure 27 (c) shows the ant tracking results in the same area, with results not as consistent as the variance or curvature attributes. In Zone A the results are more chaotic, but a N25E trend can still be deduced. This trend is also visible in other areas of the figure much like curvature. Ant tracking results from Zone do not conform to the previous fault attributes, although there is a N60E trend identified by ant tracking in other areas.

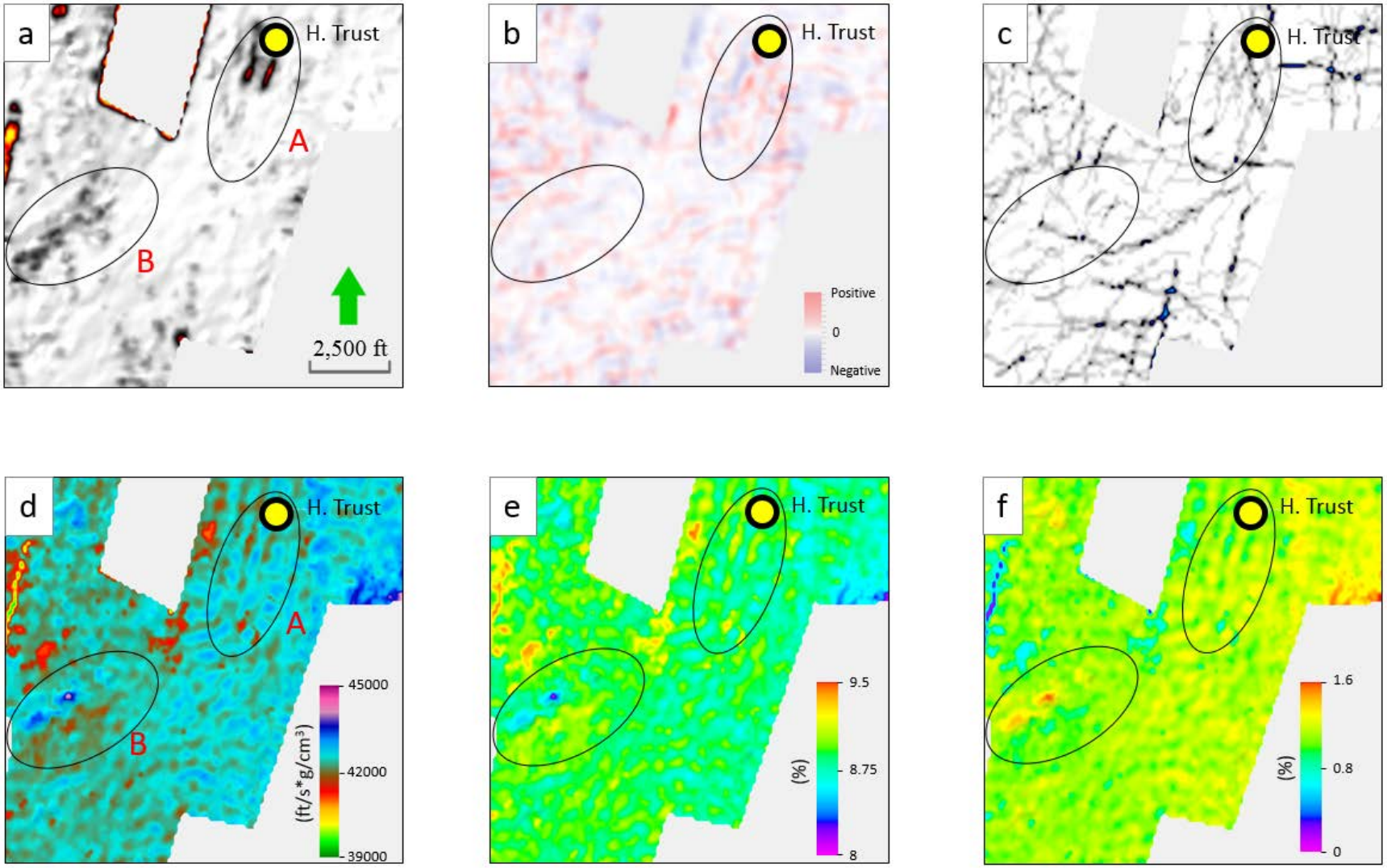

Figure 27 Comparison of fault attribute maps, AI and porosity maps of the Zone of Interest; (a) Variance, (b) Curvature, (c) Ant tracking, (d) Acoustic Impedance, (e) Total porosity and (f) Secondary porosity.

Figure 27 (d) shows the AI surface taken from the model-based inversion volume. Highest AI values are observed in Zone B, corresponding to features identified on the variance and most negative curvature displays. Values as high as 45000 ft/s*g/cm^3 are seen striking N60E. Chopra and Marfurt (2007) and others describe on the downthrown side of fault blocks, units are more brittle and greater numbers of fractures are observed. Although individual fractures cannot be resolved within the dataset, potential fracture swarms locations can be predicted based on surrounding fault behaviour.

In Zone A, a striped trend of AI is seen striking N20E. Although values do not reach as high as those observed in Zone B, a clear behaviour is seen with rapid transitions from lows of 41150 to highs of 43250 ft/s*g/cm^3. Observations were made of the relationship between AI and fault attributes.

Variance and curvature responses show a good correlation with zones of increased AI, and in turn increased secondary porosity. Similar trends are observed with ant tracking and AI, however they are not as robust. This is consistent with Figure 2 (b) where fractures are seen on the down thrown side of fault blocks. However the relationship between fault attributes and fracture porosity is qualitative, not quantitative. This is seen in Figure 27 where highest fault responses are seen in Zone A, yet highest AI and secondary porosity is seen in Zone B.

Figure 27 (e) and (f) shows total and secondary porosity of the Lower Austin Chalk respectively.

Conclusions

The current study uses 40 square miles of modern 3D seismic data to interpret horizons and faults in the Austin Chalk (AC) using amplitude, coherence, curvature and ant tracking seismic attributes. A model-based seismic acoustic impedance (AI) inversion was performed on the post stack

Pedernales PSTM seismic volume using control from the Holdsworth Trust and Holdsworth Nelson wells. This inversion method was chosen based on minimum error, and correlation between the synthetic and field trace being greater than either band limited or colored inversion. Wireline data showed good correlation between AI and sonic (matrix) porosity and neutron-density (total) porosity, respectively, in the Lower Austin Chalk. These relationships were used to calibrate the AI volume for sonic and neutron density porosity. Sonic porosity was subtracted from neutron-density porosity to establish a secondary porosity volume. Surfaces through the porosity volumes were extracted along the Lower AC over a 20 ms up window for comparison with the same surfaces extracted from the fault attribute volumes.

Variance produced the best correlation with increased secondary porosity on the Lower Austin Chalk surface of all fault attributes. Although curvature showed more detail, these additional areas identified did not correspond to significant increases in secondary porosity and led to a more chaotic display. Secondary porosity values are also shown to be independent of the magnitude of fault attribute responses, ie. Greater variance responses do not imply greater secondary porosity. Ant tracking utilizing the most positive curvature volume produced the poorest correlation with the secondary porosity of all fault attributes.

Fracture porosity values of up to 2% were identified on the downthrown side of fault blocks. Identification of fracture swarms is essential as permeability in the Austin Chalk can be increased significantly and allow communication and production from matrix pore space where hydrocarbons are held.

A workflow for evaluating secondary porosity in the Austin Chalk is presented, however the data sits several miles north of the Austin Chalk producing trend, where no AC production is documented. It is recommended that this same workflow be applied to similar data within the

producing trend. Although there are other factors that affect successful production from the Austin Chalk including hydrocarbon saturation and matrix permeability, fracture swarms are the most fundamental.

A “stacked play”, Lower Austin Chalk and Eagle Ford, would require minimal investment since modern well log and seismic data collected over the previous decade targeting the Eagle Ford, as well as infrastructure already in place on the surface to cater for Eagle Ford production has been collected and developed.

It is recommended that the Eagle Ford be evaluated further within the Pedernales survey. Production from 9 wells within the survey perimeter has been documented and dozens more in the surrounding area. All of these wells target the Lower Eagle Ford and avoid the more carbonate rich Upper Eagle Ford. An evaluation of TOC distribution and a more rigorous ant tracking investigation is recommended. Recent publications have demonstrated that applying ant tracking to specific frequency bands can improve fracture identification. By identifying such sub seismic features, migration pathways to shallower reservoirs may be identified.

References

Al-Dossary, S., Marfurt, K., 2006, 3-D volumetric multispectral estimates of reflector curvature and rotation: Geophysics, v. 71, p. 41-51

Bateman, R., 2012, Openhole Log Analysis and Formation Evaluation, 2nd ed.: Society of Petroleum Engineers.

Bahorich, M. and Farmer, S., 1995, 3-D seismic discontinuity for faults and stratigraphic features: The coherence cube: The Leading Edge, v. 14, 1053-1058

Baytok, S., 2010, Seismic investigation and attribute analysis of faults and fractures within a tight-gas sandstone reservoir: Williams Fork Formation, Mamm Creek Field, Piceance Basin, Colorado. MS thesis, University of Colorado, Boulder, CO.

Bennett, L. C., 2015, Interpretation of Late Cretaceous Volcanic Mounds and Surrounding Gulfian Series Formations Using 3D Seismic Data in Zavala County, Texas. M.S. Thesis.

Brown, A., 2011, Interpretation of Three-Dimensional Seismic Data, 7th edn. AAPG Memoir 42.

Chen, B., Kumar, D., Uerling, A., Land, S., Aguirre, O., Jiang, T. and Sugianto, S., 2015, Using seismic inversion and net pay to calibrate Eagle Ford shale resources: Interpretation, v. 3, p. 69-78.

Chopra S., Marfurt K., 2007a, Seismic attributes for prospect identification and reservoir characterization: Society of Exploration Geophysicists.

Chopra, S., Marfurt, K., 2007b, Curvature attribute applications to 3D surface seismic data: The Leading Edge, v. 26, p. 404-414.

Chopra, S., Misra, A., Marfurt, K., 2011, Coherence and curvature attributes on preconditioned seismic data: The Leading Edge, v. 30, p. 386-393.

Clemons, Kit, Hector Bello, Robert Bodziak, Matthew McChesney, Robert Meek, and Andy Stephens, 2016, Seismic attributes: Exploiting seismic data to understand heterogeneous reservoir performance in the Eagle Ford Shale, south Texas, U.S.A., in J. A. Breyer, ed., The Eagle Ford Shale: A renaissance in U.S. oil production: AAPG Memoir 110, p. 241–258.

Condon, S., Dyman, T., 2003, Geologic assessment of undiscovered conventional oil and gas resources in the Upper Cretaceous Navarro and Taylor Groups, Western Gulf Province, Texas: U. S. Geological Survey Digital Series DDS-69-H.

Corbett K., Friedman M., Spang J., 1987, Fracture development and mechanical stratigraphy of Austin Chalk, Texas: AAPG Bulletin, v. 71, p. 17–28.

Crain, E.R. 2010. Crain's Petrophysical Handbook. Mindware Ltd., Canada.

Dawson, W., 2000, Shale Microfacies: Eagle Ford Group (Cenomanian-Turonian) North-Central Texas Outcrops and Subsurface Equivalents: GCAGS, v. 50, p. 607-621.

Dawson, W.C., Katz, B., Robison, V.D., 1995, Austin Chalk petroleum system, Upper Cretaceous, southeastern Texas-A case study: GCAGS, v. 45, p. 157-163.

Dolberg, D.M., Helgesen, J., Hanssen, T.H., Magnus, I., Saigal, G. & Pedersen, B., 2000, Porosity prediction from seismic inversion, Lavrans Field, Halten Terrace, Norway. Leading Edge, 19, 392, 394, 396, 398–399.

Dravis, J.J., 1979, Sedimentology and diagenesis of Upper Cretaceous Austin Chalk Formation, south Texas and northern Mexico: Houston, Texas, Rice University, PhD dissertation.

Ewing, T. E., S. C. Caran, 1982, Late Cretaceous volcanism in south and central Texas Stratigraphic, structural, and seismic models: GCAGS, v. 32, p. 137–145.

Fang, J., Zhou, F., Tang, Z., 2017, Discrete fracture network modelling in a naturally fractured carbonate reservoir in the Jingbei oilfield, China: Energies, v. 10, p. 183.

Farghal, N. S., and M. D. Zoback, 2014, Utilizing ant-tracking to identify slowly slipping faults in Barnett Shale: Presented at the Unconventional Resources Technology Conference, SPE/AAPG/SEG.

Galloway, W.E., 2008, Depositional Evolution of the Gulf of Mexico Sedimentary Basin, in The Sedimentary Basins of the United States and Canada: New York, Elsevier, p. 505-549

Grabowski, G.J., Jr., 1984, Generation and migration of hydrocarbons in the Upper Cretaceous Austin Chalk, south-central Texas, in Petroleum geochemistry and source rock potential of carbonate rocks: American Association of Petroleum Geologists Studies in Geology no. 18, p. 97-115.

Harbor, R.L., 2011, Facies characterization and stratigraphic architecture of organic-rich mudrocks, Upper Cretaceous Eagle Ford Formation, South Texas: M.S. Thesis, The University of Texas at Austin.

Haymond, D., 1991. The Austin Chalk - an overview. Bulletin of the Houston Geological Society, v.33, p. 27-34.

Hentz, T. F., Ruppel, S. C., 2011, Regional stratigraphic and rock characteristics of Eagle Ford shale in its play area: Maverick basin to east Texas basin: Search and Discovery Article #10325

Hinds, G., and Berg, R., 1990, Estimating organic maturity from well logs, Upper Cretaceous Austin Chalk, Texas Gulf Coast: Gulf Coast Association of Geological Societies Transactions, v. 40, p. 295-300.

Hovorka, S.D., Nance, H.S., 1994, Dynamic depositional and early diagenetic processes in a deep-water shelf setting, Upper Cretaceous Austin Chalk, north Texas: GCAGS, v. 44, p. 269–276

Jacques, J. M., Clegg, H., 2002, Late Jurassic source rock distribution and quality in the Gulf of Mexico: Inferences from plate tectonic modelling: GCAGS, v. 52, p. 429-440.

Jenny, W., 1951, Aerial magnetic oil discoveries: World Oil, v. 133, no. 6, p. 85-92.

Kuich, N., 1989, Seismic fracture identification and horizontal drilling: keys to optimizing productivity in a fractured reservoir, Giddings field: Gulf Coast Association of Geological Societies Transactions, v. 39, p. 153- 157

Kumar, D., Sugianto, H., Li, S., Patel, H., Land S., 2014, Using relative seismic impedance to predict porosity in the Eagle Ford shale: SEG Technical Program Expanded Abstracts, 2688-2692, doi: 10.1190/segam2014-0473.

Lancaster, S. and D. Whitecombe, 2000, Fast-track Coloured Inversion: SEG expanded abstract, doi: 10.1190/1.1815711.

Latimer, R. B., Davison, R., Riel, P. V., 2000, An interpreter's guide to understanding and working with seismic-derived acoustic impedance data: The Leading Edge, 19, No. 3, 242–256.

Lindseth, R. O., 1979, Synthetic sonic logs—a process for stratigraphic interpretation. Geophysics, v. 44, p. 3-26. doi:10.1190/1.1440922

Liner, C. 2016, Elements of 3D seismology. Society of Exploration Geophysicists.

Martin, R., Baihly, J., Malpani, R., Lindsay, G., Atwood, W.K, 2011, Understanding Production From Eagle Ford-Austin Chalk System. Presented at the SPE Annual Technical Conference and Exhibition, Denver, 30 October–2 November. SPE-145117 MS.

Martinez-Torres, Liliana Patricia. Characterization of naturally fractured reservoirs from conventional well logs. Diss. University of Oklahoma, 2002.

Mathews, T.F., 1986, The petroleum potential of 'serpentine plugs' and associated rocks of central and south Texas: Baylor Geological Studies, v. 68, p. 504.

Najmuddin, I. J., 2003, Austin chalk fracture mapping using frequency data derived from seismic data. Doctoral dissertation, Texas A&M University.

Ogiesoba, O.C., Eastwood, R., 2013, Seismic multiattribute analysis for shale gas/oil within the Austin Chalk and Eagle Ford Shale in a submarine volcanic terrain, Maverick Basin, South Texas. Interpretation, p. 61–83.

Pearson, K., 2012, Geologic models and evaluation of undiscovered conventional and continuous oil and gas resources—Upper Cretaceous Austin Chalk, U.S. Gulf Coast: U.S. Geological Survey Scientific Investigations Report 2012–5159, 26 p.

Pedersen-Tatalovic, R., Uldall, A., Jacobsen, N., Hansen, T., Mosegaard, K., 2008, Event-based low-frequency impedance modeling using well logs and seismic attributes: The Leading Edge, v. 27, no. 5, p. 592–603.

Roberts, A., 2001, Curvature attributes and their application to 3D interpreted horizons: First Break, v. 9, p. 85-100. doi:10.1046/j.0263-5046.2001.00142.

Robison, C.R., 1997. Hydrocarbon source rock variability within the Austin Chalk and Eagle Ford Shale (Upper Cretaceous), East Texas, U.S.A. International Coal Geology, 34; 287-305.

Russell, B., and D. Hampson, 1991, A comparison of post-stack seismic inversion methods: 61st Annual International Meeting, SEG, Expanded Abstracts, 876–878.

Russell, B.H., 1988, Introduction to seismic inversion methods. Society of Exploration Geophysicists.

Salvador, A., ed., 1991, Origin and development of the Gulf of Mexico basin, in The Gulf of Mexico Basin: Boulder, Colo., Geological Society of America, Geology of North America, v. J, p. 389-444.

Schlanger, S.O., Jenkyns, H.C., 1976, Cretaceous oceanic anoxic events: causes and consequences: Geol. Mijnbouw, v.55, p. 179-184.

Schnerk, G. C., and C. N. Madeen, 2000, The Austin Chalk: Simulation of horizontal wells in a heterogeneous formation: Society of Petroleum Engineers, SPE 20716.

Scholle, P.A., 1977, Chalk diagenesis and its relation to petroleum exploration: Oil from chalk, a modern miracle?: AAPG Bulletin, v. 61, p. 982-1009.

Scott, R. J., 2004, The Maverick Basin: New Technology-New Success: Gulf Coast Association of Geological Societies Transactions, v. 54, 603- 620.

Smirnov, Andrey, 2018, Interpretation and Fracture Characterization of Early-Cretaceous Buda Limestone Formation Using Post-Stack 3D Seismic Data in Zavala County, Texas: Theses and Dissertations. 2629.

Snyder, H., R, and Craft, J. M., 1977, Evaluation of Austin and Buda Formations from Core and Fracture Analysis: ABSTRACT. AAPG Bulletin, 61.

Stapp, W., 1977, Geology of Fractured Austin Chalk and Buda Limestone in South Texas: AAPG Bulletin, v. 27, p. 208-229.

Treadgold, G., McLain, B., Sinclair, S., 2011, Eagle Ford Shale Prospecting with 3D Seismic Data: Proc. of Society of Economic Geologists Annual Meeting, Denver, 2270-2273.

Tyler, N., Ambrose, W.A., 1986, Depositional systems and oil and gas plays in the Cretaceous Olmos Formation, south Texas: Austin, Tex., University of Texas, Bureau of Economic Geology Report of Investigations no. 152. v. 40, p. 295-300.

Winter, J.A., 1961, Stratigraphy of the lower Cretaceous (subsurface) of South Texas: Gulf Coast Association of Geological Societies, v. 11, p. 15-24.

Appendix A

Stephens Production Company provided precomputed sonic porosity values for both the Holdsworth Nelson and Holdsworth Trust. When these original sonic porosity values were plotted vs N-D porosity (Figure 27), they plot significantly below the equity line suggesting that matrix porosity is greater than total porosity. Since this is not possible the sonic log was investigated further.

The distribution of the original sonic porosity values in the Lower Austin Chalk (Figure 28) shows an average of 10.49% for the Holdsworth Trust and 14.8% for the Holdsworth Nelson. These values are higher than is reported in the literature.

Pyrite, which has been observed in the Eagle Ford and Austin Chalk (Grabowski, 1984), and other heavy minerals, can can adversely affect sonic log measurements. A cross plot of Photoelectric Effect and density in the LAC was used to test if any such minerals were present, with negative results (Figure 29). Each well was then evaluated individually.

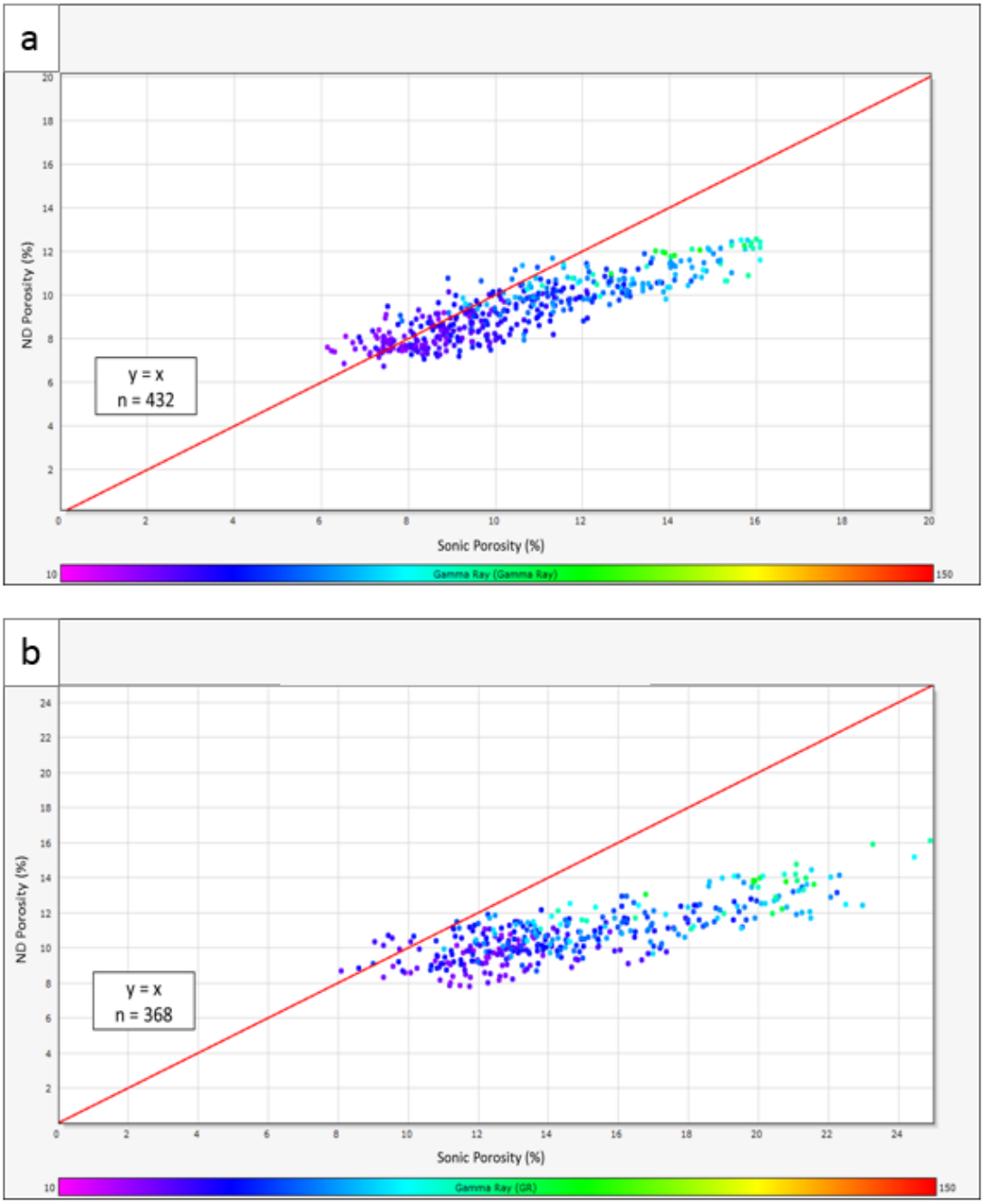

Figure 27. Original Sonic porosity values in the Lower Austin Chalk of the (a) Holdsworth Trust and (b) Holdsworth Nelson. The majority of data points plot below the equity line, implying matrix porosity is greater than total porosity.

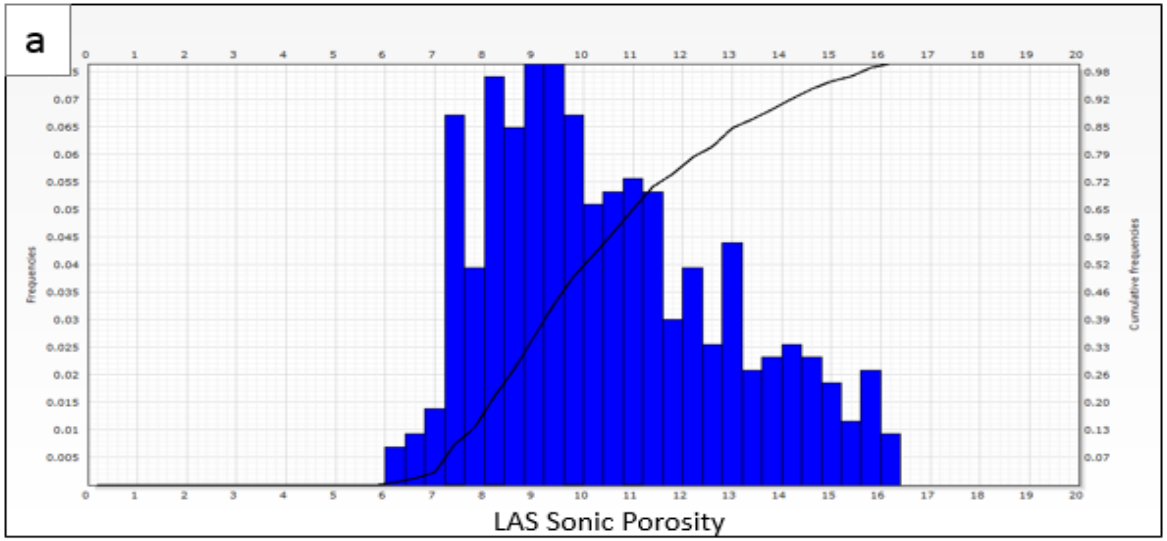

Statistic	(%)
Mean	10.49
Mode	9.2
Standard Deviation	2.35
Minimum Value	6.146
Maximum Value	16.09

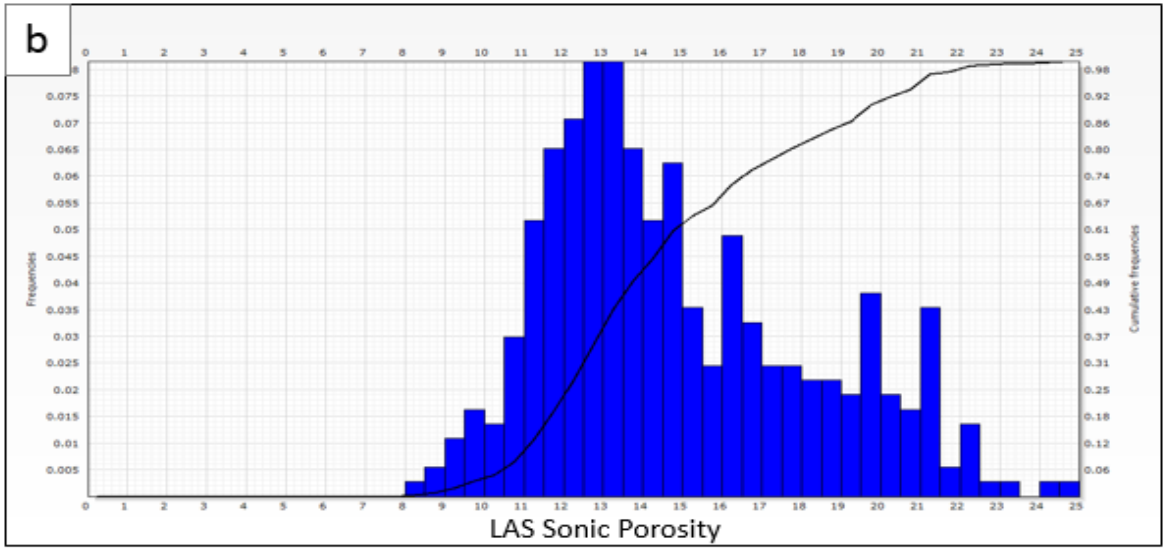

Statistic	(%)
Mean	14.87
Mode	13
Standard Deviation	3.35
Minimum Value	8.081
Maximum Value	24.91

Figure 28. Distribution of sonic porosity values in the (a) Holdsworth Trust and (b) Holdsworth Nelson. Average matrix porosities are much higher than those listed in the literature.

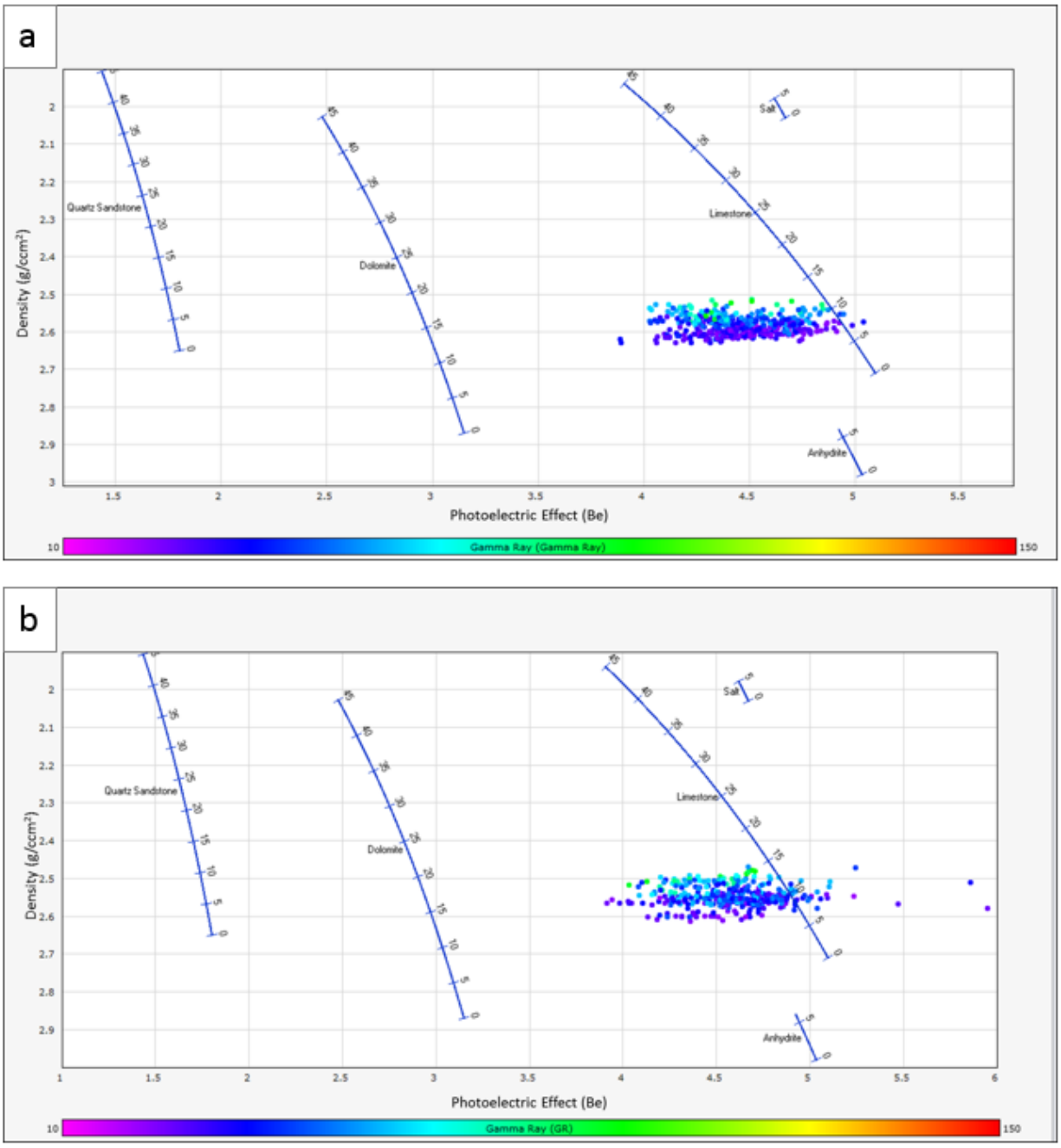

Figure 29. Cross plot of Photoelectric Effect and Density of the Lower Austin Chalk in the (a) Holdsworth Trust and (b) Holdsworth Nelson. This is typically used to identify heavy minerals, which have been shown to distort sonic porosity readings. No such minerals were identified.

Holdsworth Trust

The Holdsworth Trust caliper was first assessed. Throughout the entire AC and EF interval, the borehole shows consistent shape, with no evidence of washout or mudcaking.

Although a sonic porosity log was provided, the method used to calculate these numbers from the primary sonic data was not given. The Wylie time average equation was used as described previously (Asquith and Krygowski, 2004), with values generated within 1% of the original sonic porosity values.

Bateman (2012) describes several environmental factors that can inflate sonic porosity measurements, one of which is the hydrocarbon effect. Since no mudlogs were available for the vertical well, the density and neutron porosity log overlay was used. No cross over was observed (Figure 23) suggesting that neither gas nor oil was present in the formation and the hydrocarbon effect was not the cause of increased sonic porosity values.

Bateman (2012) also refers to the effect of shale on sonic porosity measurements, however closer examination of Figure 27 shows the over compensated sonic porosity is not specific to higher GR zones indicating presence of shale. The full spectrum of GR values is seen below the equity line from clean carbonate to muddy carbonate to carbonate mud.

The effect of under compaction causes sonic porosity values to be over stated (Bateman, 2012). Under compaction is defined where velocities of more than 100 μs/ft are observed in shale rich zones on the sonic log. Because the LAC and MAC do not contain any pure shale intervals, this was originally overlooked. However, shale pulses are seen in the UAC and significant shale is present in the overlying Anacacho where velocities recorded in these zones do exceed 100 μs/ft. The closest shale interval, (as determined by the shale line on the GR log), was seen at 5230.5 ft

and is approximately 2 ft thick. Austin Chalk sonic porosity values were corrected using the compaction correction to the Wylie equation;

$$\emptyset_S = \frac{t_{log} - t_{ma}}{t_f - t_{ma}} \frac{1}{C_p}$$

Where:

$$C_p = \mathrm{c}\frac{t_{sh}}{100}$$

Where:

c = shale compaction coefficient, typically assigned a value of 1

t_{sh} = sonic log measurement in overlying shale zones

Holdsworth Nelson

A similar procedure was followed for Holdworth Nelson well. Again, the caliper was checked showing a consistent borehole size. No mudlog was available for the vertical well like the Holdsworth Trust, with the results of the density neutron log overlay suggesting the hydrocarbon effect is not the cause of increased sonic porosity values.

Thin shale beds in the Upper Austin Chalk and Anacacho Limestone were observed with velocities of greater than 100 µs/ft from 4475 to 4500 ft MD. The Holdsworth Nelson sonic porosity values were then corrected for under compaction.

To assess the accuracy of the corrected sonic log values, nearby data was investigated. No relevant sonic log or core data from the survey area was found in the Texas Railroad Commission and IGOR (Integrated Core and Log Database, Bureau of Economic Geology-University of Texas) databases. As a result data from outside the survey was considered. Because Gulfian rocks dip

basin ward and matrix porosity is a function of depth (Dravis, 1979), samples to the north and south were not investigated.

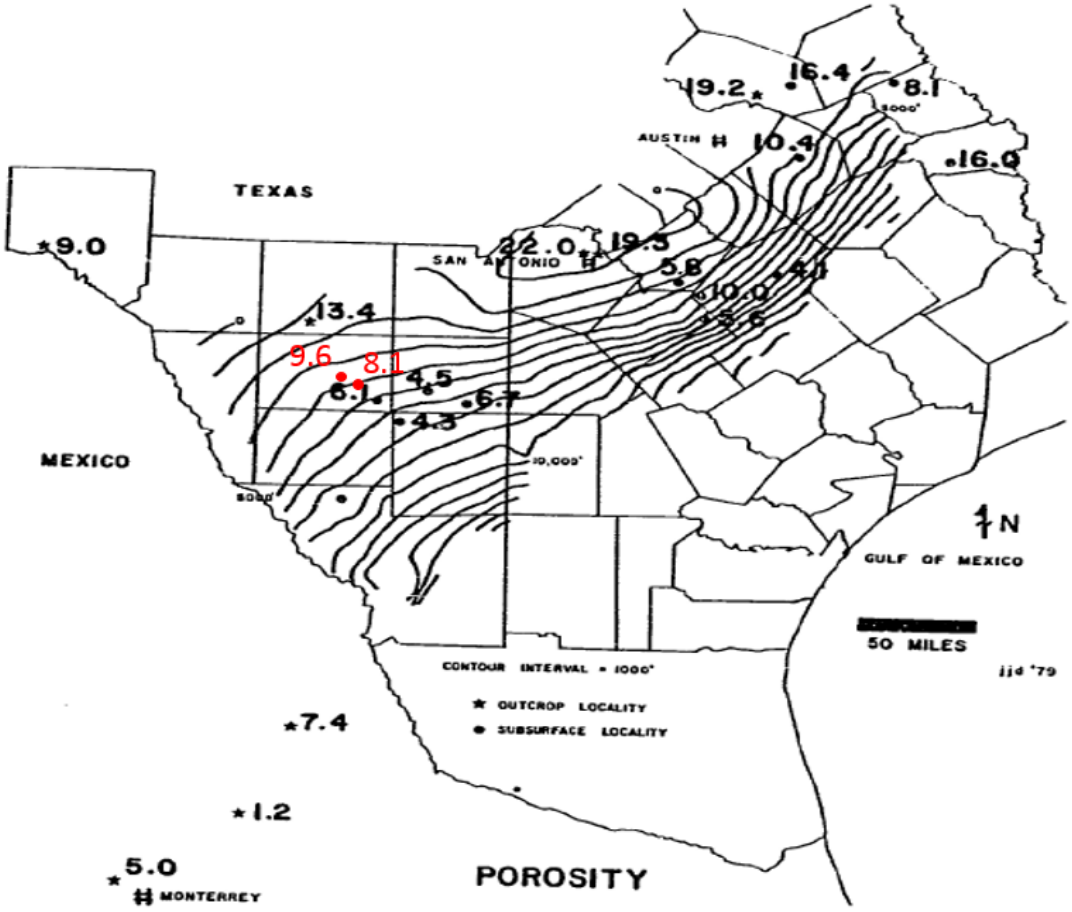

Figure 30. Dravis (1979) plotted average matrix porosity values of the Austin Chalk recovered from wireline readings, core measurements and thin sections. The corrected matrix porosity of the entire AC interval is plotted in red of the Holdsworth Trust and Holdsworth Nelson, which appears to show a good fit with the trend identified. Modified from Dravis (1979).

The closest core measurements available are from the Winterbotham well (Figure 29), where Dravis (1979) uses these and other core measurements from the surrounding counties to describe the trend of decreasing matrix porosity values with depth. This was the only measurement available within a radius of 20 miles from the perimeter of the survey.

Dravis (1979) uses values recovered from the entire Austin Chalk interval, not just the Lower Austin Chalk as is in this investigation. The approximate location of the Holdsworth Nelson and Holdsworth Trust well are annotated on Figure 29, with the average sonic porosity of the entire AC interval also included. The two corrected sonic porosity points appear to fit the trend identified by Dravis (1979) better than the original AC average sonic porosity values of 10.1% for the Holdsworth Trust and 12.8% for the Holdsworth Nelson.

Appendix B

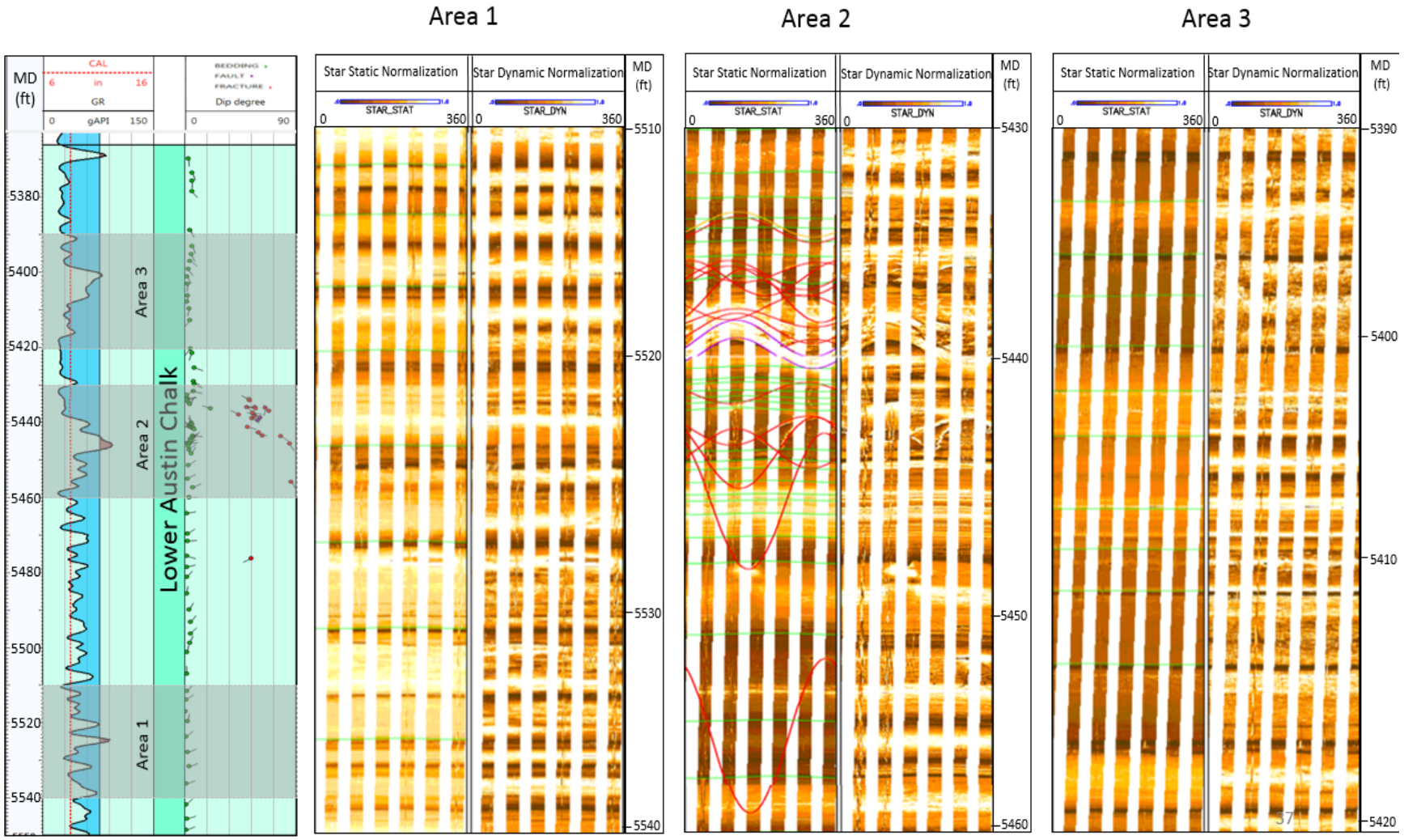

Figure 31. Results of the FMI log in the Holdsworth Nelson well. The FMI shows a greater level of detail than the GR curve, emphasizing how laminated the AC interval is. Fractures and faults do not appear to be restricted to particular lithological zones, while vugs can also be seen.